Karlsruhe Institute of Technology

Same-sign top signals at the LHC within the flavour violating MSSM

Diplomarbeit
von

Yasmin Claire Anstruther

An der Fakultät für Physik
Institut für Theoretische Physik

Referent: Prof. Dr. D. Zeppenfeld
Korreferent: Prof. Dr. M. Mühlleitner

April 2012

Ich versichere, dass ich diese Arbeit selbstständig verfasst und ausschließlich die angegebenen Hilfsmittel verwendet habe.

Yasmin Claire Anstruther
Karlsruhe, den 13. April 2012

Als Diplomarbeit anerkannt.

Prof. Dr. D. Zeppenfeld
Karlsruhe, den 13. April 2012

Zusammenfassung

Die vorliegende Arbeit befasst sich mit der Phänomenologie der flavourverletzenden Supersymmetrie. Flavourverletzung bezeichnet hierbei die Option bei einer Teilchenwechselwirkung verschiedene Teilchengenerationen zu mischen. Die Frage, ob nicht-minimale Flavourverletzung im Rahmen der Supersymmetrie am LHC sichtbar ist oder nicht, soll anhand einer durch Monte Carlo Simulationen erarbeiteten Analyse geklärt werden. Dazu wurde ein Prozess gewählt, der auf der Identifikation von Bottom-Quarks beruht. Diese Identifikationsmethode wird b-Tagging genannt und ist gut erprobt. Der Prozess, welchen wir genauer untersucht haben, beinhaltet im Endzustand zwei Bottom-Quarks, zwei Leptonen gleicher Ladung und fehlende Transversalenergie. Der Endzustand wird durch zwei Top-Quarks produziert, welche wiederum durch Squark-Paarproduktion über den Austausch eines Gluinos im t-Kanal erzeugt wurden, $pp \to 2t + 2\chi_1^0 \to 2b + 2l^+ + E_{miss}^T$.

Das Standardmodell der Teilchenphysik ist inzwischen eine wohletablierte Theorie. Sie vereint drei der vier fundamentalen Wechselwirkungen, nämlich die elektromagnetische, die schwache und die starke Kraft. Im Vergleich zu diesen dreien ist die Gravitation bei kurzen Abständen sehr schwach und infolgedessen vernachlässigbar. Mit dem Standardmodell kann man äußerst präzise Vorhersagen machen. Dennoch ist es nicht zufriedenstellend. Es kann zum Beispiel nicht erklären, woraus dunkle Materie besteht. Ferner kann es das sogenannte Hierarchieproblem der Korrekturen zur Higgsmasse nicht bändigen. Vor allem letzteres wies auf die Idee einer Supersymmetrie hin, indem man zusätzliche Teilchen mit einem anderen Spin einführt, die mit der gleichen Kopplungsstärke wechselwirken, wie ihr Partnerteilchen im Standardmodell.

Supersymmetrie ist als eine Erweiterung des bekannten Standardmodells anzusehen. Grundlegende Konzepte, wie beispielsweise die störungstheoretische Beschreibung von Streuprozessen, können weiterhin angewendet werden. Sie postuliert infolge der Beschreibung durch graduierte Lie Algebren zwar neue Teilchen, aber keine neuen Wechselwirkungen. Supersymmetrietransformationen überführen Fermionen in Bosonen und umgekehrt. Kommutator- und Antikommutatorrelationen aus diesen und den Erzeugenden der Poincaré Algebra verknüpfen Supersymmetrie mit Raumzeit Symmetrien. Dies gliedert sich in die Formulierung des Standardmodells über lokale Eichgruppen ein. Das minimale supersymmetrische Standardmodell, kurz MSSM, ist aus phänomenologischer Sicht am zugänglichsten, da es lediglich 105 neue, unbekannte Parameter besitzt. Zwei davon werden in dieser Arbeit studiert, zum einen die "RR 13" und zum anderen die "LR 13" Mischung zwischen Squarkflavoureigenzuständen. Diese Parameter entstehen auf natürliche Weise durch die Brechung von Supersymmetrie. Solch ein Brechungsmechanismus ist erforderlich, da exakte Supersymmetrie zu einer Entartung

der standardmodellartigen Teilchenmassen und deren supersymmetrischen Partnern führt. Da bisher keine dieser neuen Teilchen beobachtet wurden, muss man annehmen, dass diese Supersymmetrie gebrochen ist. Die Einführung eines weich brechenden Potentials führt auf (6×6)-dimensionale Massenmatrizen, welche eine zusätzliche Flavourverletzung, jenseits der CKM-Mischung, ermöglichen.

Nicht-minimale Flavourverletzung verkompliziert die Berechnung von Wirkungsquerschnitten, da Mischungsmatrizen höherer Dimension und zusätzliche Übergänge beitragen können. Die Mischung zwischen der zweiten und dritten Teilchengeneration wurde in [3] studiert. Es wurde herausgefunden, dass die Wirkungsquerschnitte für $pp \to c\bar{t}(t\bar{c}) + E^T_{miss} + X$ im Bereich von $\mathcal{O}(100\text{ fb})$ bei einer Schwerpunktsenergie von 14 TeV und einer integrierten Luminosität von 100 fb^{-1} liegen können. Eine detaillierte Monte Carlo Analyse wurde jedoch nicht präsentiert. In [2] wurde die Mischung zwischen der ersten und dritten Generation bei der Higgsproduktion in Betracht gezogen. Wiederum ermöglicht diese Option der Mischung von Teilchengenerationen die simultane Produktion zweier Top-Quarks gleicher Ladung durch Squarkpaarproduktion, wie sie an folgendem Feynman Diagramm dargestellt wird. Der Endzustand weist zwei Bottom-Quarks und zwei positiv geladene Leptonen, sowie einen fehlenden Transversalimpuls auf.

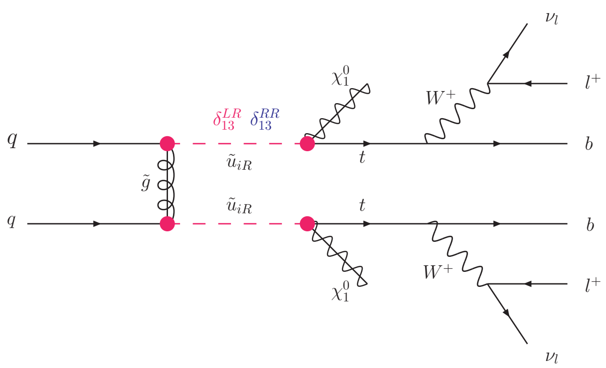

Die flavourverletzenden Parameter beeinflussen auch andere Observablen. Dazu gehören in erster Linie der elektroschwache $\rho-$Parameter, sowie Prozesse flavourverändernder neutraler Ströme. Letztere sind Gegenstand der sogenannten $B-$Physik. Diese Observablen wurden bereits gemessen [38] und die durch flavourverletzende Parameter erzeugte Abweichung muss im Rahmen der Messgenauigkeit liegen. Des Weiteren haben aktuelle Suchen nach Squarks am LHC Ausschlussgrenzen bezüglich deren Massen ergeben. Diese liegen jedoch unterhalb eines TeVs und stehen einer Analyse mit Squarkmassen um 1 TeV nicht im Wege. Durch unsere letztendliche Wahl der Parameter wird eine Masse des leichtesten, Standardmodell artigen Higgses von 125 GeV generiert. Dies stimmt mit aktuellen Messungen der Experimente CDF, DØ [42], ATLAS und CMS [43] überein. Aus theoretischer Sicht müssen Bedingungen bezüglich der Stabilität des Vakuums erfüllt sein. Diese resultieren aus der Forderung, dass die Minima des weich brechenden supersymmetrischen Potentials, wie gewohnt, Ladung und Farbe erhalten. Wenn alle Nebenbedingungen erfüllt sind, so ist der von uns gewählte Parameterpunkt noch nicht ausgeschlossen.

Das oben genannte Signal wird über die Paarproduktion zweier Squarks durch den Austausch eines Gluinos im t-Kanal ermöglicht. Die Squarks zerfallen anschließend weiter, jeweils in ein Quark und ein Neutralino. Dieses Neutralino ist das leichteste und somit ein stabiles supersymmetrisches Teilchen unseres Modells. Dies ermöglicht es ihm als Kandidat für dunkle Materie zu fungieren. Ziel ist es, möglichst viele Top-Quarks zu erzeugen. Dies gelingt indem man den Mischungsparametern der Matrix der weich brechenden Massen entsprechende nicht-diagonale Werte zuweist. In unserem Fall sind es die Einträge $(\mathcal{M}_{\tilde{u}}^2)_{16}, (\mathcal{M}_{\tilde{u}}^2)_{46}$ und $(\mathcal{M}_{\tilde{u}}^2)_{64}$, wobei die beiden letzteren identisch sind, weil die Matrix hermitesch ist. Diese Einträge entsprechen der Mischung zwischen der ersten und dritten Teilchengeneration zwischen links- und rechtshändigen beziehungsweise nur zwischen rechtshändigen Squarks. Sie werden beschrieben durch die dimensionslosen Parameter δ_{13}^{LR} und δ_{13}^{RR}. Genau diese beiden Parameter sind relevant, um ein möglichst rechtshändiges Squark im Zwischenzustand zu erzeugen, sodass dieses hauptsächlich in ein Top-Quark und das leichteste Neutralino zerfällt. Das Neutralino ist eine Mischung aus Bino, Wino und Higgsinos. Als leichtestes Neutralino ist der Bino Anteil am größten und letzteres koppelt nur an rechtshändige Teilchen. Da sich im Proton sowohl links- als auch rechtshändige Quarks befinden, wird neben der "RR" Mischung auch "LR" benötigt. Durch die Variation dieser beiden oben genannten Parameter soll der totale Wirkungsquerschnitt $\sigma(pp \to tt\chi_1^0\chi_1^0)$ maximiert werden, um das bestmögliche Szenario für eine Analyse zu finden. Im Detail wurden drei verschiedene Szenarien untersucht. Zuerst wurde eines mit sehr ähnlichen Werten zu [3] betrachtet. Danach erhöhten wir die Massen der Squarkmasseneigenzustände auf etwa 1 TeV und untersuchten zwei verschiedene Hierarchien. Zuletzt erzeugten wir ein Spektrum, wie man es in effektiven supersymmetrischen Theorien vorfindet. Das bedeutet, dass die dritte Generation der Squarks wesentlich leichter ist, als die Squarks der ersten und zweiten Teilchengeneration. Der dabei resultierende Wirkungsquerschnitt ist jedoch so klein, dass er am LHC nicht wird gemessen werden können. Daher entschieden wir uns für Parameter des Szenarios (B) mit absteigender Hierarchie der Diagonalelemente der Massenmatrix $\mathcal{M}_{\tilde{u}}^2$.

Die Analyse des Prozesses $pp \to 2t + 2\chi_1^0 \to 2b + 2l^+ + E_{miss}^T$ erfordert die Berücksichtigung aller möglichen Untergründe. Dazu gehöhren sowohl standardmodellartige als auch supersymmetrische Reaktionen, die den gleichen Endzustand produzieren wie das Signal, also zwei Bottom-Quarks, zwei positiv geladene Leptonen und fehlender Transversalimpuls. Die Topologien der supersymmetrischen Hintergrundreaktionen entsprechen der des Signals. Allerdings handelt es sich dabei um die Produktion leichter Quarks, die vom Detektor versehentlich als Bottom-Quarks identifiziert werden können. Im Rahmen des Standardmodells kann die gewünschte Signatur in den Kanälen $t\bar{t}W^+$, W^+W^+jj und W^+Zjj hervorgebracht werden. Die Untergründe können auf zwei Arten reduziert werden: Zum einen durch b-Tagging und zum anderen durch Einschränkungen des Phasenraums, sogenannte Cuts. Neben den üblichen kinematischen Cuts, eignet sich vor allem der durch $t\bar{t}W^+$ induzierte Untergrund für zusätzliche Cuts. Die Untergründe und deren Reduktion werden in Kapitel 6 ausführlich diskutiert.

Wir haben die Analyse für die Parameter $(\delta_{13}^{RR}|\delta_{13}^{LR}) = (0.803|0.055)$ einmal bei einer Schwerpunktsenergie von 7 TeV mit einer integrierten Luminosität von 30 fb^{-1} und bei 14 TeV mit 100 fb^{-1} durchgeführt. Die Verteilung des transversalen Impulses zeigt, dass das Signal weitgehend gegenüber dem Untergrund dominiert. Es wurden nur sehr wenige Ereignisse erzeugt und folglich eine Signifikanz von $1,05\sigma$ erreicht. Den größten Beitrag zum Untergrund liefert die $t\bar{t}W^+$ Produktion. Da bislang noch keine ausgereifte Methode zur Unterscheidung zwischen Bottom-Quarks und deren Antiquarks existiert, wurden die vom $\bar{t}$ ausgehenden $\bar{b}$ als b identifiziert. Dieser Untergrund läst sich möglicherweise durch die Unterscheidung von b und $\bar{b}$ deutlich reduzieren. Der Schritt zu einer Schwerpunktsenergie von 14 TeV und 100 fb^{-1} ergab folgendes: Es konnten sowohl mehr Ereignisse erzeugt als auch eine Signifikanz von $2,46\sigma$ erzielt werden. Trotz dieser Verbesserung stieg das Signal relativ zum supersymmetrischen Untergrund weniger an. Der gesamte supersymmetrische Untergrund stieg dreimal so stark an wie das Signal, wohingegen der Standardmodell artige Untergrund etwas weniger als das Signal zunahm. Es ist daher anzunehmen, dass die Analyse des Prozesses $pp \to 2t + 2\chi_1^0 \to 2b + 2l^+ + E_{miss}^T$ für Squarkmassen im Bereich von einem TeV eine verhältnismäßig geringe Schwerpunktsenergie von 7 TeV und viel an integrierter Luminosität erfordert.

Zuletzt wurde ein Vergleich zwischen einem flavourerhaltenden und einem flavourverletzenden Szenario erarbeitet. In [3] wurde der Anstoß gegeben, flavourverletzende Kanäle bei der Suche nach Squarks am LHC miteinzubeziehen. Wir haben dies für unseren Prozess betrachtet, und zwar unter der Annahme von Mischungen zwischen der ersten und dritten Teilchengeneration. Dazu verzichteten wir auf das b-Tagging und untersuchten den Endzustand bestehend aus zwei Quark-Jets, zwei positiv geladenen Leptonen und fehlendem Transversalimpuls. Im Gegensatz zu den oben genannten Analysen, stammt der größte Untergrundbeitrag von der W^+W^+jj Produktion. Was das Signal betrifft, so konnten durch Flavourverletzung etwas mehr Ereignisse generiert werden als ohne. Zudem werden die sich im Endzustand befindlichen Bottom-Quarks als Ausschlag im unteren Bereich der Verteilung des Transversalimpulses sichtbar. Dieser ist im flavourerhaltenden Fall nicht vorhanden. Insgesamt betrachtet sind dies nur kleine Änderungen im Verlauf der Histogramme. Des Weiteren konnte im flavourerhaltenden Fall eine Signifikanz von $3,41\sigma$ und im flavourverletzenden Fall $3,95\sigma$ erzielt werden.

Die Ergebnisse können folgendermaßen zusammengefasst werden: Sollte Supersymmetrie am LHC entdeckt werden, dann ist es wichtig, die Parameter der Theorie möglichst präzise zu bestimmen. Die Analysen in den Kapiteln 6.3 und 6.4 können dabei behilflich sein um die Flavourverletzung jenseits der CKM-Mischung zu erforschen, insbesondere wenn die Unterscheidung zwischen Bottom-Quarks und deren Antiteilchen möglich ist. Da eine solche Flavourverletzung durch die Brechung der Supersymmetrie induziert wird, kann man aus den Messergebnissen möglicherweise Rückschlüsse auf den bisher unbekannten Brechungsmechanismus ziehen.

Danksagung

Zuallererst möchte ich mich bei Herrn Prof. Dr. Dieter Zeppenfeld für die angenehme Betreuung sowie für Korrekturvorschläge bezüglich dieser Arbeit bedanken. Ferner danke ich ihm auch dafür, dass er mir das interessante und vielfältige Thema zur Erforschung vorschlug. Des Weiteren bedanke ich mich für das Ermöglichen der Teilnahme an der LPPP11 Herbstschule in Freiburg und das Vortragen meiner Ergebnisse auf der Frühjahrstagung der DPG in Göttingen.

Ebenfalls möchte ich mich bei Frau Prof. Dr. Margarete Mühlleitner herzlich bedanken, dass sie sich bereit erklärte das Korreferat zu übernehmen.

Bei meinem Betreuer Dr. Michael Rauch möchte ich mich besonders dafür bedanken, dass er jederzeit bereit war, meine Fragen verschiedenster Art ausführlich zu beantworten. Er war es auch, der das Thema dieser Diplomarbeit anregte.

Darüber hinaus bedanke ich mich für eine angenehme Atmosphäre und viele fruchtbaren Diskussionen am Insitut. Ebenfalls danke ich allen, die Teile dieser Arbeit Korrektur lasen: Bastian Feigl, Jessica Frank, Matthias Kerner, Eva Popenda, Dr. Michael Rauch, Christian Röhr, Martin Stoll, Juraj Streicher, Kathrin Walz, sowie Peter Anstruther für sprachliche Hilfestellungen.

Ein großer Dank geht an meine Eltern Brigitte und Peter Anstruther, sowie an meine Großeltern Erika und Wilhelm Wolf, die mich moralisch und finanziell während des Studiums unterstützten.

Zu guter letzt möchte ich mich bei meinem Freund Alexander Heß für seine liebevolle Zuneigung während des gesamten Studiums zutiefst bedanken.

Contents

CHAPTER 1

Introduction

Ever since the ancient Greeks, physics, especially particle physics, has the intention to "... perceive whatever holds the world together in its innermost folds" [1]. Whether or not this is possible and what would happen after achieving this knowledge, is a very philosophical issue. The fact that the interest in this subject seems to be time-independent and substantial progress has been achieved, especially during the last fifty years, justifies the efforts in particle physics enormously.

Quantum mechanics were discovered during the beginning of the 20th century and describe physics at low energies. Physics at high energies require a relativistic formulation of quantum theory as to which O. Klein, W. Gordon and P. Dirac contributed. Particles and their interactions can be described by a quantisation of fields, e.g. photons are the quanta and mediator particles of the electromagnetic field. Three out of four interactions, to be specifically the strong, weak and electromagnetic, can be described within the Standard Model (SM), see Chapter 2. As gravity is known to be very weak at small distances, it can be neglected for the time being. Despite the success of the Standard Model, it may not be the most suited theoretical approach to nature. Within Chapter 3 we will discuss open issues, which can not be explained by the Standard Model. Many theories beyond the Standard Model adress these problems, e.g. supersymmetry.

Supersymmetry combines space-time symmetries with internal symmetries. This requires a supersymmetric partner to each Standard Model particle. If supersymmetry is not broken, the masses of the Standard Model particles and their supersymmetric partners would be degenerate. The fact that we have not yet observed any of these partner particles leads to the assumption that supersymmetry, if it is realized in nature, must be broken. This leads to the issue of breaking mechanisms and in turn to a source of flavour violation beyond the well-known quark mixing in the SM. This additional mixing is known as non-minimal flavour violation. The supersymmetry breaking terms contain parameters which have an impact on the masses and the mixing of squarks.

At the moment the Large Hadron Collider (LHC) at the "Centre Européen pour la Recherche Nucléaire" (CERN) is operating at the centre-of-mass energy of 7 TeV and achieved an integrated luminosity of more than 5 fb^{-1}. In 2014 a centre-of-mass energy of 14 TeV is expected to be reached and after this, hopefully soon, data corresponding to 100 fb^{-1} can be taken into account. To date, no evidence as to wheter supersymmetry can be used as an accurate description of nature has been discoverd. A lot of effort has been put into studying this theory and its phenomenology precisely. This work should tie in with existing studies and concentrate on the possibiliy of non-minimal flavour violation, specialised within the squark sector.

We study the signal process containing two bottom quarks originating from two top quarks, two same-sign leptons and missing transverse energy in the final state: $pp \to 2t + 2\chi_1^0 \to 2b + 2l^+ + E_{miss}^T$ at leading order. Due to the fact, that we have external supersymmetric particles, in our case the stable lightest neutralino χ_1^0, non-minimal quark flavour violation can already occur at tree-level. Compared to processes containing solely internal supersymmetric particles in loops, we expect sizable effects, because the process is not suppressed by the typical loop factor of $\frac{1}{16\pi^2}$.

The effect of non-minimal flavour violation within the minimal supersymmetric Standard Model has been studied in various publications, e.g. [2, 3]. However, mainly mixing between the second and third generation was taken into account. This is often explained by an analogy to the largest off-diagonal entry of the CKM matrix in the Standard Model. Anyway, there is no explicit reason, why mixing between the second and third generation should be larger than mixing among the first and third generation. We are considering same-sign top production via squark pair production, which can be enhanced by mixing between the first and third generation. However, the mixing parameters can not be chosen arbitrarily large. The choice of these parameters also has an effect on other observables. Among these are flavour changing neutral current transitions from B-Physics, as well as processes, which serve as discovery channels for squarks at the LHC. Vacuum stability conditions constrain the mixing parameters, from theory, to adhere the conservation of charge and colour. These constraints are discussed in Chapter 4 in order to assure that our flavour violating parameters have not yet been excluded.

Chapter 6 is addressed to a Monte Carlo based analysis of the signal $pp \to 2t + 2\chi_1^0 \to 2b + 2l^+ + E_{miss}^T$. First, we identify the possible background processes, stemming from the Standard Model on the one hand, and from supersymmetry on the other. The Standard Model processes $t\bar{t}W^+$ and $VVjj$, with V being either a W^+ boson or a Z boson, result in the same signature as the signal. The Feynman diagrams corresponding to the background from supersymmetry have the same topology as the signal process. The production of bottom quarks is a characteristic of the signal process. As bottom quarks are much heavier than down, up, strange and charm quarks and therefore have a shorter lifetime, they can be tagged to certain efficiencies. B-tagging can reduce the background tremendously, because the background processes mainly produce very light quarks, which are only taken into account if they have been mis-tagged. Another method to reduce the background is to apply cuts. Some cuts, e.g. transverse momentum cuts, are necessary because the detector does not enclose the beam pipe. Particles escaping in this direction have to be added to the missing transverse momentum of the event. Other cuts, e.g. related to the invariant mass of a bottom quark and a lepton, reduce the background, especially from $t\bar{t}W^+$. Besides this, a jet veto considering additional jets, originating from the W^- boson, reduces the $t\bar{t}W^+$ background further. We perform an analysis at the centre-of-mass energy of 7 TeV with an integrated luminosity of 30 fb^{-1} and at 14 TeV with 100 fb^{-1}.

Finally, we study whether or not non-minimal flavour violation has an effect on current searches for squarks, as suggested in [3]. For this purpose we abandon b-tagging and study the signal $pp \to 2j + 2l^+ + E^T_{miss}$, produced via flavour violating and via flavour conserving squark pair production, respectively.

CHAPTER 2

Passing the Standard Model

2.1 Motivation

The first idea of, what is known as the Standard Model (SM) evolved during the 1960's when e.g. M. Gell-Mann and G. Zweig introduced the idea of quarks[1], as constituents of hadrons [4,5] and when A. Salam and S. Weinberg described how to unify the electromagnetic and weak force [6,7]. Many predictions as the existence of the top quark as well as asymptotic freedom of strong interactions have been verified, which make the SM a reliable theory within its limits. We will discuss limits and problems later during the motivation of supersymmetry. For more details the reader is refered to [8,9].

2.2 Elementary Particles and Interactions

At the moment the number of elementary particles, i.e. particles without any substructure, which have been discovered, is quite manageable. They can be seen as quanta of a quantised field, either fermionic or bosonic. By assuming gauge invariance of the theory, terms that represent the observed interactions arise in the Lagrangian, the starting point of a physical model. This will be explained briefly in this Chapter.

Symmetries and Symmetry breaking

Today we know of four fundamental interactions: strong, electromagnetic, weak and gravitational. The SM is able to describe the first three of these by using group theory methods. Such as assuming gauge invariance to assure spatial independence of the theory and requires extra terms, combined in a covariant derivative besides the free fields. As the interactions do not influence each other, the SM gauge group can be written as a direct product:

$$\mathrm{SU}(3) \times \mathrm{SU}(2) \times \mathrm{U}(1). \tag{2.1}$$

[1] At the time, sometimes called ”aces”.

The dimension of a Lie group SU(N) is N^2-1, which corresponds to the number of generators. The product's dimension is the sum of the generators of each group $8+3+1=12$. The commutator relations

$$[T^a, T^b] = i\sum_{i=1}^{8} f^{abc}T^c, \tag{2.2}$$

$$[I^a, I^b] = 2i\sum_{i=1}^{3} \varepsilon^{abc}I^c \tag{2.3}$$

of their generators $T^a = \lambda^a/2$, $a = 1, ..., 8$ of the SU(3) and $I^a = \sigma^a/2$, $a = 1, 2, 3$ of the SU(2) and the phase α of the abelian U(1) generate the Lie algebras with the structure constants f^{abc} for SU(3) and ε^{abc} for SU(2). λ^a and σ^a denote the Gell-Mann and Pauli matrices, respectively. The covariant derivatives, e.g. $\mathrm{D}_\mu = \partial_\mu - ig_s G^a_\mu \frac{\lambda^a}{2}$, contain the generators and in this case the gluon field G^a_μ. Therefore, the dimension of the Lie group is equal to the number of particles. In our case we have one photon γ, three weak bosons $W^\pm, Z$ and eight gluons g.

The following table shows the particle content of the SM [10]:

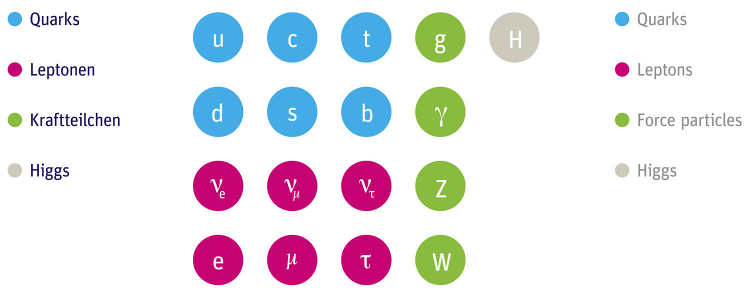

Figure 2.1: SM particles, the first three columns contain fermions and represent the three generations. The fourth column shows the gauge bosons and the last one contains the scalar Higgs field.

In detail, the $W^\pm$, Z and γ bosons are compositions of the gauge fields $W^\mu_{1,2,3}$ and B^μ, corresponding to the groups SU(2) and U(1) after the SU(2) $\times$ U(1) symmetry has been spontaneously broken down to the $\mathrm{U_{em}}(1)$. The rotation angle θ_W which mixes the original states is called the Weinberg angle.

$$\begin{pmatrix} A_\mu \\ Z_\mu \end{pmatrix} = \begin{pmatrix} \cos\theta_W & -\sin\theta_W \\ \sin\theta_W & \cos\theta_W \end{pmatrix} \begin{pmatrix} B_\mu \\ W^3_\mu \end{pmatrix} \tag{2.4}$$

$$W^\pm_\mu = \frac{1}{\sqrt{2}}(W^1_\mu \mp iW^2_\mu) \tag{2.5}$$

Spontaneous symmetry breaking means that the Lagrangian has a symmetry which the ground state of the potential is not subjected to anymore. This happens at the scale of about 100 GeV by assigning a non-zero vacuum expectation value (vev) to the Higgs field, which is described by a scalar field H. Its potential reads:

$$V_{\mathrm{SSB}}(H) = \mu^2|H|^2 + \lambda|H|^4 \tag{2.6}$$

with $\lambda > 0$ to assure a lower bound of the energy and $\mu^2 < 0$ to assure the existence of a minimum, $\lambda, \mu^2 \in \mathbb{R}$. Its minimum is located at $H_0 = \sqrt{-\frac{\mu^2}{2\lambda}} e^{i\theta}$, where the arbitrary phase $0 \leq \theta \leq 2\pi$ is a continuous parameter and generates degenerate ground states. The easiest choice is $\theta = 0$ and leads to $H_0 = v/\sqrt{2}$ with the non-zero vev $v := \sqrt{-\frac{\mu^2}{2\lambda}}$. Unphysical degrees of freedom can be eliminated by choosing e.g. the unitary gauge. Going through this procedure, fermions, as well as W and Z bosons gain mass. The gauge boson masses result from the kinetic terms $(D_\mu H)(D^\mu H)$. Fermion masses are proportional to the Yukawa coupling y and come from Yukawa terms, which have a $y\psi\bar{\psi}H$ structure. To date, this Higgs boson remains the only undiscovered particle of the SM, although it was already predicted as far back as 1964 [11–13]. Concluding, we can write down the Lagrangian density for the electroweak sector of the SM as follows:

$$
\begin{aligned}
\mathcal{L}_{\text{SM}} =& \mathcal{L}_{\text{kin}} + \mathcal{L}_{\text{SSB}} + \mathcal{L}_{\text{Yukawa}} + \mathcal{L}_{\text{gauge}} \qquad (2.7) \\
=& i(\bar{Q}_i^\alpha \gamma^\mu D_\mu Q_i^\alpha + \bar{u}_{Ri}^\alpha \gamma^\mu \tilde{D}_\mu u_{Ri}^\alpha + \bar{d}_{Ri}^\alpha \gamma^\mu \tilde{D}_\mu d_{Ri}^\alpha + \bar{L}_i \gamma^\mu D_\mu L_i + \bar{l}_{Ri} \gamma^\mu \tilde{D}_\mu l_{Ri}) \\
&+ (D_\mu H)^\dagger (D^\mu H) - \mu^2 H^\dagger H - \frac{\lambda}{4}(H^\dagger H)^2 \\
&- (Y_{ij}^U \bar{Q}_i^\alpha H^C d_{uj}^\alpha + Y_{ij}^D \bar{Q}_i^\alpha H d_{Rj}^\alpha + Y_{ij}^L \bar{L}_i H l_{Rj} + h.c.) \\
&- \frac{1}{4}(B_{\mu\nu} B^{\mu\nu} + W_{\mu\nu}^a W^{a\mu\nu}) \qquad (2.8)
\end{aligned}
$$

with the following notation of covariant derivatives and fields, etc:

$$
\begin{aligned}
D_\mu =& \partial_\mu + igW_\mu^a t^a + ig' B_\mu \frac{Y}{2} \\
\tilde{D}_\mu =& \partial_\mu + ig' B_\mu \frac{Y}{2}
\end{aligned}
\qquad
\begin{aligned}
B_{\mu\nu}, W_{\mu\nu}^a &: \text{field strength tensors} \\
Y_{ij} &: \text{non-diagonal Yukawa matrices}
\end{aligned}
$$

and the fermionic left handed SU(2) doublets $Q = (u, d)^T$ and $L = (l, \nu)^T$, the right-handed singlets u_R, d_R, l_R, and the bosonic Higgs field H, its charge conjugated field H^c and the gauge boson fields B_μ of U(1), W_μ^a of SU(2) with $a = 1, 2, 3$ and the the gauge couplings g' and g, respectively. Y denotes the hypercharge and the index α denotes the colour, which is the conserved quantity due to the SU(3) invariance.

S-Matrix and Cross Sections

The probability amplitude $\mathcal{M}_{fi}$ of scattering or transitions of particles is described by the S-Matrix. It transfers the asymptotic initial $|i\rangle = |\phi(t = -\infty)\rangle$ to the final state $|f\rangle = |\phi(t = \infty)\rangle$.

$$
t = -\infty \quad |i\rangle \quad \rightarrow S \rightarrow \quad |f\rangle \quad t = \infty \qquad (2.9)
$$

It is the solution to the Schrödinger equation $i\partial_t |\phi(t)\rangle = H_W(t)|\phi(t)\rangle$:

$$
S = Te^{i \int \mathcal{L}_W(x) d^4x} \qquad (2.10)
$$

with the time-ordering operator T and the Hamiltonian H_W, which is responsible for interactions and can be derived from the Lagrangian density. Unfortunately, these Green's functions have not been derived and we have to be satisfied with an expansion of the exponential function in small couplings contained in $\mathcal{L}_W$.

Using Wick's theorem the terms of these perturbation series can be expressed by means of Feynman rules, which will be used in the following calculations, see e.g. Figure 5.2 in Chapter 5.

A full hadronic cross section σ is obtained in two steps. First, the perturbative so-called partonic cross section $\hat{\sigma}$ has to be derived e.g. for two incoming partons m and n according to Equation:

$$\begin{aligned}\hat{\sigma}_{mn} &= \frac{1}{\sqrt{(p_m p_n)^2 - m_m^2 m_n^2}} \int d(\mathrm{LIPS}) |\mathcal{M}_{fi}|^2 \\ &= \frac{1}{\sqrt{(p_m p_n)^2 - m_m^2 m_n^2}} \int (2\pi)^4 \delta^{(4)}(P_f - P_i) \prod_f \frac{d^3 p_f}{(2\pi)^3 2 p_f^0} |\mathcal{M}_{fi}|^2,\end{aligned} \tag{2.11}$$

containing the prefactor before the integral as flux factor, the Lorentz-invariant phase space $d(\mathrm{LIPS})$ and the squared matrix element $|\mathcal{M}_{fi}|^2$. The capital letters P_f, P_i denote the sum of final and initial momenta, respectively. The initial particles of this hard process are partons, the constituents of the proton. Their behaviour has to be described non-perturbatively by parton distribution functions (PDF), because their momentum transfer Q^2 of about 100 GeV^2 is quite low. The perturbative and non-perturbative parts of an hadronic cross section are separated at the factorisation scale μ_F. Analogously to the RGEs one can write down DGLAP[2] Equations to study the dependence on μ_F:

$$\mu_F \frac{df_{m/P}(x_m, \mu_F)}{d\mu_F} = \sum_k P_{m/k} \otimes f_{k/P}(x_k, \mu_F), \tag{2.12}$$

with the convolution $[f \otimes g](x) := \int_0^1 \int_0^1 dydz f(y) g(z) \delta(x - yz)$, the Altarelli-Parisi splitting kernels $P_{m/k}$ and the PDFs $f_{k/P}$. At an absolute value, e.g. $\mu_F = m_Z$ the PDFs are fitted to experimental data. By using the DGLAP Equations (2.12) they can be evolved to any arbitray scale. The splitting functions are the anomalous dimensions of the DGLAP equations. They are used e.g. by the Monte Carlo event generator Herwig++ [52] within the parton shower and in higher order matrix elements. At leading order the PDFs can be interpreted as the probability of finding one of the light quarks (d, u, s, c, b) inside the proton. Despite the naive picture of valence quarks $\{u, d\}$ and gluons g forming a proton, vacuum polarisations contain loops of virtual quarks, which are known as sea quarks. Every parton has its own PDF, which is derived by a fit to experimental data at a fixed scale and can not be written as an analytic function. There are many groups providing sets of PDFs and we have used MRST 2007 lomod (LO* for MC) [60]. Now we can calculate the hadronic cross section by a convolution with the luminosity functions $\frac{d\mathcal{L}_{mn}}{d\tau}(\tau, \mu_F^2) = \int_0^1 dx_m \int_0^1 dx_n f_{m/P}(x_m, \mu_F^2) f_{n/P}(x_n, \mu_F^2) \times \delta(\tau - x_m x_n)$:

$$\sigma = \sum_{m,n} \int_{\tau_0}^1 d\tau \frac{d\mathcal{L}_{mn}}{d\tau}(\tau, \mu_F^2) \hat{\sigma}_{mn}(\tau s, \mu_F^2). \tag{2.13}$$

with the partonic center of mass energy $\sqrt{\hat{s}} := \sqrt{\tau s}$ and the threshold production energy $\sqrt{\tau_0 s}$. The momentum fraction of the partons m, n are given by x_m and x_n. This concept and more details are explained in [14].

[2]Dokshitzer–Gribov–Lipatov–Altarelli–Parisi.

2.3 Flavour violation in the SM

Flavour violation is a characteristic of the electroweak gauge group SU(2)×U(1) and its spontaneous symmetry breaking. Therefore it only occurs within gauge and Yukawa interactions of left- and right-handed fermions. We restrict ourselves to the quark sector because we will refer to this later. The interaction terms of the Lagrangian density read:

$$\begin{aligned} -i\mathcal{L}_{\text{interaction}} =& i(\bar{Q}_i\gamma^\mu D_\mu Q_i + \bar{u}_{Ri}\gamma^\mu \tilde{D}_\mu u_{Ri} + \bar{d}_{Ri}\gamma^\mu \tilde{D}_\mu d_{Ri} && (2.14)\\ & - (Y^U_{ij}\bar{Q}^\alpha_i (H^C)^\alpha u_{Rj} + Y^D_{ij}\bar{Q}^\alpha_i H^\alpha d_{Rj}) - h.c. && (2.15)\end{aligned}$$

As a result of the spontaneous symmetry breaking explained above, the mass terms for the quarks have the following form:

$$\mathcal{L}_{\text{mass}} = -vY^U_{ij}\,\bar{u}^i_L u^j_R - vY^D_{ij}\,\bar{d}^i_L d^j_R \qquad (2.16)$$

containing again the Yukawa coupling matrices, which can be diagonalised by a rotation from the interaction or flavour basis $\{u^o, d^o\}$ to the basis of physical mass eigenstates $\{u, d\}$. To do this simultaneously with both matrices, two unitary transformations are necessary:

$$u_{L/R} = V^u_{L/R} u^o_{L/R} \qquad\qquad d_{L/R} = V^d_{L/R} d^o_{L/R} = (V_{CKM} V^u_{L/R}) d^o_{L/R} \qquad (2.17)$$

with $V_{CKM} := V_u^\dagger V_d$ being the Cabbibo-Kobaysahi-Maskawa matrix[3] (CKM matrix), which contains all information about flavour and CP violation in the Standard Model. The elements are given either directly, in terms of the weak mixing angles θ_{12}, θ_{13}, θ_{23} and a complex phase δ or as an expansion in $\lambda = \sin\theta_{12} := s_{12} \approx |V_{us}|$ up to λ^3, which has been named after L. Wolfenstein:

$$\begin{aligned} V_{CKM} &= \begin{pmatrix} V_{ud} & V_{us} & V_{ub} \\ V_{cd} & V_{cs} & V_{cb} \\ V_{td} & V_{ts} & V_{tb} \end{pmatrix} && (2.18)\\ &= \begin{pmatrix} c_{12}c_{13} & s_{12}c_{13} & s_{13}e^{-i\delta} \\ -s_{12}c_{23} - c_{12}s_{23}s_{13}e^{i\delta} & c_{12}c_{23} - s_{12}s_{23}s_{13}e^{i\delta} & s_{23}c_{13} \\ s_{12}s_{23} - c_{12}c_{23}s_{13}e^{i\delta} & -c_{12}s_{23} - s_{12}c_{23}s_{13}e^{i\delta} & c_{23}c_{13} \end{pmatrix} && (2.19)\\ &= \begin{pmatrix} 1-\frac{\lambda^2}{2} & \lambda & A\lambda^3(\rho - i\eta) \\ -\lambda & 1-\frac{\lambda^2}{2} & A\lambda^2 \\ A\lambda^3(1-\rho-i\eta) & -A\lambda^2 & 1 \end{pmatrix} + \mathcal{O}(\lambda^4) && (2.20)\end{aligned}$$

with $A\lambda^2 = s_{23}$ and

$$s_{13}e^{i\delta} = A\lambda^3(\rho + i\eta) = \frac{A\lambda^3(\bar{\rho} + i\bar{\eta})\sqrt{1 - A^2\lambda^4}}{\sqrt{1-\lambda^2}[1 - A^2\lambda^4(\bar{\rho} + i\bar{\eta})]}, \qquad (2.21)$$

where $\bar{\rho} + i\bar{\eta} = -(V_{ud}V^*_{ub})/(V_{cd}V^*_{cb})$. These formulae assure unitarity to all orders and $\delta \neq 0$ corresponds to CP-violation. The CKM elements have been measured [15] with the result, that the diagonal entries predominate the off-diagonal entries which correspond to mixing between several generations.

[3]In agreement with the Les Houches Accord 2 convention, whereas the PDG defines $V_{CKM} = V_u^{PDG}(V_d^{PDG})^\dagger$, with $V_u^{PDG} = (V_u^{LHA2})^\dagger$ and $V_d^{PDG} = (V_d^{LHA2})^\dagger$.

The following work has been performed by using the Wolfenstein parameters from the Particle Data Group [15] as input values, where we have neglegted CP violation to simplify the interpretation of upcoming mixing matrices in Chapter 5:

A	λ	$\bar{\rho}$	$\bar{\eta}$
$0.8116^{+0.0097}_{-0.0241}$	$0.22521^{+0.00082}_{-0.00082}$	$0.139^{+0.025}_{-0.027}$	0

Table 2.1: Wolfenstein parameters.

CHAPTER 3

Concepts of Supersymmetry

3.1 Motivating Physics beyond the Standard Model

Despite the success the SM has already achieved, it is a theory which is not valid to arbitrary high energies. Today the LHC is about to explore higher energies than ever before and new phenomena might not be describable by the SM. Besides this, experiments from cosmology have posed new issues like dark matter and dark energy. Unfortunately, its composition is still unknown. Even theoretical problems are present in the framework of the SM, e.g. if one calculates corrections to the Higgs mass. The following Chapter should point out that supersymmetry might be a possible answer to these issues and therefore worth studying, although there are, as yet no direct hints to its phenomenology. On top of this, the minimal supersymmetric Standard Model (MSSM), surprisingly, leads to the unification of the three gauge couplings.

Unification

In the SM we have seen, that the electromagnetic and weak theory unify at the weak scale of around 100 GeV. Supersymmetry is thought of as a theory which describes nature at the TeV scale, then energies are high enough to produce supersymmetric particles.
Unfortunately, the parameters of our Lagrangian turn out to be unphysical when calculating higher orders. To rescue the physicalness a procedure named renormalisation has to be applied. In doing so a new scale, called the renormalisation scale, has to be introduced. After calculating an observable to all orders of perturbation theory the renormalisation scale should cancel out again. The dependence of physical parameters on this scale is governed by the renormalisation group equations, presented later in Equations (4.2) and (4.4). Hence, a calculation of higher orders requires the calculation of corrections to quantities as e.g. the couplings. The dependence on the scale Q is referred to as the running of the couplings and is presented in Figure 3.1, [16].

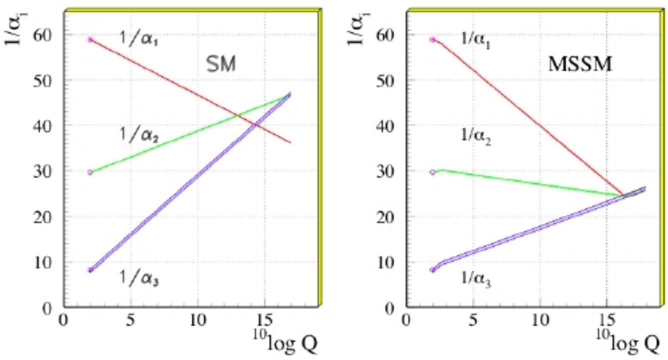

Figure 3.1: Unification of gauge couplings in the SM and MSSM.

In the case of supersymmety, new particles can be produced mainly as virtual states at about 1 TeV. These additional particles have been taken into account as threshold corrections and alter the curves, so that they luckily meet at the scale of so-called Grand Unification (GUT). No experimental evidence for the unification of these three couplings exists but it has been a wishful thinking since the time of A. Einstein.

Furthermore the SM only describes three of four known interactions, as gravity is not included. This is mainly due to two facts. On the one hand gravity is much weaker than the other forces and on the other hand it is not renormalisable, which makes the approach of perturbation theory useless. However, one big aim in theoretical particle physics is a theory containing all four interactions, which is possible in M-theory with supersymmetry as prior condition. Unfortunately, the phenomenology of string theories is hardly elaborated.

Dark Matter

In 1937 F. Zwicky postulated dark matter (DM) as some kind of mass to explain the observation that the velocity of rotating galaxies does not decrease when going radially outwards [17]. Recent studies [18] claim, that the total energy of our universe consists of 23% DM and only 4.6% of baryonic matter. An astonishing 72% are dark energy (DE) which drives the expansion of the universe. The matter distribution of today and 13.7 billion years ago is shown in Figure 3.2, [18]. Possible descriptions of this DE are e.g. energy densities like Einstein's Cosmological Constant or a scalar field filling the universe [19], [20].

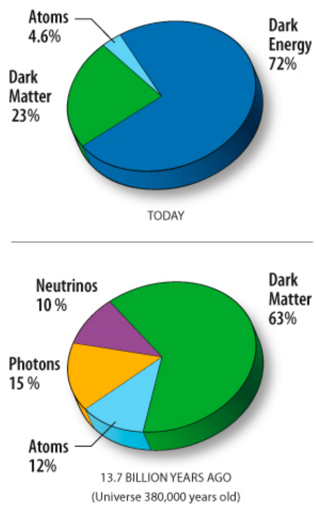

Figure 3.2: Content of the universe.

Today many other experimental results can be very well measured by including DM and DE. This is especially the case for the measurement of the cosmic microwave background radiation (CMB) performed by the Wilkinson Microwave Anisotropy Probe (WMAP). It shows the remaining radiation stemming from the big bang which occurred approximately 13.7 billion years ago [21].

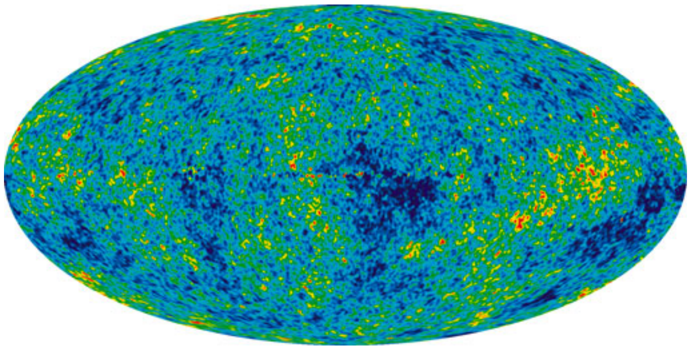

Figure 3.3: Cosmic microwave background radiation measured by the WMAP satellite during a 7 year period.

Unfortunately, what DM consists of is an unsolved mystery. In contrast to baryonic DM, which is disfavoured by the primordial nucleosynthesis, R-Parity conserved SUSY promotes a stable candidate for cold non-baryonic DM, the so-called lightest supersymmetric particle (LSP). It merely interacts weakly and gravitationally and therefore, is undetectable and must be studied e.g. via the distribution of missing transverse momenta. As we will see in Chapter 6.

Hierarchy Problem

The SM only makes sense, when the origin of masses can be explained and the most promising way, is to postulate a Higgs boson which arises through spontaneous symmetry breaking. The Higgs is a massive particle itself and therefore quantum corrections to its mass can be calculated, which are important for its potential discovery at the LHC. The first order correction to the scalar mass is

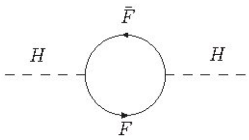

$$\delta m_s^2 = -\frac{\lambda_F^2}{8\pi^2}\left[\Lambda^2 - m_F^2 \ln \frac{\Lambda^2}{m_F^2}\right] \quad (3.1)$$

Figure 3.4: Feynman diagram of a SM correction to the Higgs mass.

where λ_F denotes the fermionic coupling, m_F the mass of the fermion running in the loop and Λ the so-called cut-off parameter, which indicates the maximum possible scale up to which the theory is valid. When taking gravity into account this is the Planck scale at $\mathcal{O}(10^{19})$ GeV and the mass correction becomes very large because of the Λ^2-term, while physical processes are expected at the weak scale of $\mathcal{O}(10^3)$ GeV. This discrepancy of 16 orders of magnitude is the actual hierarchy problem and sometimes referred to as an aesthetical issue. The logarithmic dependence on Λ cab be absorbed in the counter term after renormalisation. The problematic quadratic divergence can be canceled by taking supersymmetric particles into account. This leads to the following contribution including the scalar coupling λ_S:

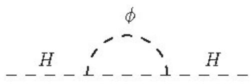

Figure 3.5: Feynman diagram of a SUSY correction to the Higgsmass.

$$\delta m_{s'}^2 = +\frac{\lambda_S^2}{8\pi^2}\left[\Lambda^2 - m_\phi^2 \ln\frac{\Lambda^2}{m_\phi^2}\right] \tag{3.2}$$

By adding up both corrections under the simple supersymmetric assumption $\lambda_F = \lambda_S$ the quadratic divergences drop out. If the scalar mass m_ϕ is of $\mathcal{O}(1)$ TeV no further fine tuning is necessary. Incidentally, this complication does not occur when one calculates the corrections to the masses of the gauge bosons and fermions, because they are protected by gauge and chiral symmetries, respectively.

Neutrino Oscillations

Last but not least, the discovery of neutrino oscillations in 1998 made it clear, that not everything can be predicted by the SM. Within the SM neutrinos are massless but the oscillation probability contains the difference of neutrino mass squares $\Delta m^2 = m_i^2 - m_j^2$ of two generations $\{i, j\}$. In the two flavour formalism it is:

$$P(\nu_i \leftrightarrow \nu_j) = \sin^2(2\theta)\sin^2\left(\frac{\Delta m^2 L}{4E}\right) \tag{3.3}$$

where θ denotes the weak mixing angle, L the flight distance and E the kinetic energy. Similar to the mixing in the quark sector via the CKM matrix, this mixing of lepton flavour can be described by the Pontecorvo-Maki-Nakagawa-Sakata (PMNS) matrix.

More detailed information about these motivating issues can be found in [19,20,22–25]. Next, we will turn to the basic idea of supersymmetry.

3.2 Supersymmetry and the MSSM

Taking advantage of symmetries, simplifies a lot of problems in physics. According to Noether's first theorem, every continuous symmetry transformation is correlated to a conservation law. In this Chapter a new symmetry called supersymmetry (SUSY) will be introduced.

Idea

A SUSY transformation Q turns bosonic into fermionic states and vice versa:

$$Q|B\rangle \rightarrow |F\rangle, \tag{3.4}$$

$$Q|F\rangle \rightarrow |B\rangle. \tag{3.5}$$

The couplings are equal, which solves the hierarchy problem, described above. Furthermore the masses of particles and their superpartners will initially be degenerate and form a so-called multiplet. The theory called the MSSM, is not an entirely new theory, it ought to be thought of a supersymmetrised SM. So the theory should, live in four space time dimensions, be Poincaré invariant and respect internal gauge symmetries. Now, supersymmetry means to combine space time symmetries with gauge symmetries in a non-trivial way. If only compact Lie algebras are taken into account, this was proven to be impossible by S. Coleman and J. Mandula in 1967. Only the possibility of a direct product between the Poincaré group and compact Lie groups exists, but no other combination, so that general assumptions [26], e.g. about the S-matrix are fulfilled. This makes it a "no-go" theorem. By then, basic theories e.g. by J. Wess and B. Zumino were already established and it took seven years, before R. Haag, J. Lopuszanski and M. Sohnius could show, that there is a way to construct a superalgebra [27].

The Coleman-Mandula theorem can be invalidated by enlarging the Poincaré algebra with anti-commutation relations of the SUSY generators Q to a superpoincaré algebra generated by [28]:

$$
\begin{aligned}
[P^\mu, P^\nu] &= 0 && (3.6)\\
[P^\mu, M^{\rho\sigma}] &= i(g^{\mu\rho}P^\sigma - g^{\mu\sigma}P^\rho) && (3.7)\\
[M^{\mu\nu}, M^{\rho\sigma}] &= -i(g^{\mu\rho}M^{\nu\sigma} - g^{\mu\sigma}M^{\nu\rho} - g^{\nu\rho}M^{\mu\sigma} + g^{\nu\sigma}M^{\mu\rho}) && (3.8)\\
[P^\mu, Q^1_a] &= [P^\mu, Q^1_{\dot a}] = 0 && (3.9)\\
[M^{\mu\nu}, Q_a] &= -\Sigma^{\mu\nu}_{ab} Q_b && (3.10)\\
\{Q^1_a, \bar{Q}_{\dot b 1}\} &= 2\gamma^\mu_{a\dot b} P_\mu && (3.11)
\end{aligned}
$$

where 1 denotes a phenomenological viable ($\mathcal{N} = 1$) SUSY and $\gamma^\mu_{a\dot b}$ the Pauli matrices, generalised to four dimensions. The Weyl indices $a, b \in \{1, 2\}$ transform under the $(0, \frac{1}{2})$ Poincaré group representation, and $\dot a, \dot b \in \{1, 2\}$ under $(\frac{1}{2}, 0)$. Mathematically, this is a Z_2 graduated Lie algebra. The four components of P^μ generate translations, the six independent components of $M^{\mu\nu}$ generate rotations and boosts. The first three equations induce the simple Poincaré algebra. Equation (3.9) leads to degeneration of the masses $m_F = m_B$. The anti-commutator, Equation (3.11) is proportional to the generator of translations and makes the connection to space-time symmetries and what is more even gravity.

That the number of fermions must equal the number of bosons can be derived by using Equation (3.11) and the Wittenindex $\Delta = \mathrm{tr}(-1)^{N_F}$, where N_F denotes the fermion number operator. The Wittenindex gives the difference between the number of fermionic and bosonic states:

$$\Delta\{Q, \bar{Q}\} = 0 \Leftrightarrow \Delta = 0 \Leftrightarrow \#B = \#F. \tag{3.12}$$

Particles are described by irreducible representations of the SUSY algebra, which are classified into multiplets, corresponding to mass and superspin (m, y). There exist two types of multiplets: vector supermultiplets with superspin $y = \frac{1}{2}$ and chiral supermultiplets with $y = 0$. According to the quantum numbers, mass and superspin the particles can be arranged into supermultiplets.

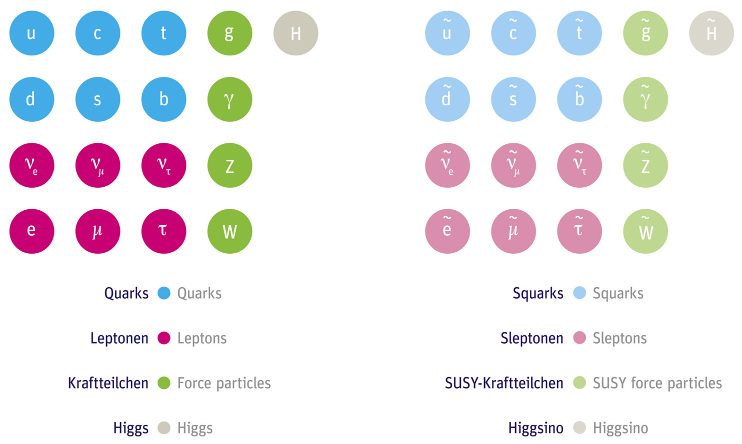

Figure 3.6: The blue, pink and gray particles belong to chiral supermultiplets with $y = 0$, whereas all green particles are described by vector supermulitplets with $y = \frac{1}{2}$.

The superspin y dictates the eigenvalues of Casimir operators and therefore identifies the irreducible representations. All superfields are described within the superfield formalism as finite power series in supercoordinates $(x_\mu, \theta, \bar{\theta})$, where θ and $\bar{\theta}$ are anti-commuting Grassmann variables

$$\begin{aligned}\Phi(x,\theta,\bar{\theta}) =& f(x) + \theta\phi(x) + \bar{\theta}\bar{\chi}(x)\\ &+ \theta\theta m(x) + \bar{\theta}\bar{\theta}n(x) + \theta\gamma^\mu\bar{\theta}v_\mu(x)\\ &+ \theta\theta\bar{\theta}\bar{\lambda}(x) + \bar{\theta}\bar{\theta}\theta\psi(x) + \theta\theta\bar{\theta}\bar{\theta}d(x). \end{aligned} \tag{3.13}$$

MSSM

The simplest phenomenologically viable supersymmetric theory is the MSSM, which postulates the fewest additional particles to the SM. This includes two Higgs doublets H_1 with hypercharge $Y = -1$ and H_2 with $Y = 1$ to keep the theory free of anomalies and ensure an analytic superpotential. Two types of superfields, expanded in terms of Grassman variables are necessary as irreducible representations of the SUSY algebra, namely chiral and vector superfields. Vector superfields are real and are formed as a product of a chiral superfield and its hermitian conjugate. A chiral superfield must solve $D_{\dot{\alpha}}\Phi(x_\mu, \theta, \bar{\theta}) = 0$, where $\dot{\alpha}$ denotes the Weyl spinor index transforming under the $(\frac{1}{2}, 0)$ representation of the Poincaré group.

Up to now, we were always assuming an exact supersymmetry, which postulates new particles with exactly the same mass as their partners. If this was true, we would have been able to see them at, e.g. the Tevatron or LEP. Consequently, if we do not want to give up this theory, we can assume that supersymmetry is broken at our present scale. As we want the part of the Lagrangian $\mathcal{L}_{\text{SUSY}}$ to be invariant under supersymmetry transformations, this breaking must have been soft in some kind of ”hidden” sector and then somehow transfered to the ”visible” sector. How this works is very speculative, but there are some common ideas like gauge mediation (GMSB) or gravity mediation (mSUGRA). This part of the Lagrangian we call $\mathcal{L}_{\text{SOFT}}$ and thus the Lagrangian density of the MSSM can be decomposed into the following parts:

$$\mathcal{L}_{\text{MSSM}} = \mathcal{L}_{\text{SUSY}} + \mathcal{L}_{\text{SOFT}} + \mathcal{L}_{\text{GAUGE-FIX}} + \mathcal{L}_{\text{GHOST}}. \tag{3.14}$$

The largest part to derive is $\mathcal{L}_{\mathrm{SUSY}}$ and because it is not necessary for the understanding of the following work we refer to [29]. The gauge-fixing and ghost terms are analogous to the SM. Most important for the following work is the soft breaking term $\mathcal{L}_{\mathrm{SOFT}}$. In general $\mathcal{L}$ must be:

- renormalisable, i.e. the mass dimension of each term must be at most equal to four,
- SUSY and SU(3) $\times$ SU(2) $\times$ U(1) invariant,
- baryon number minus lepton number (B-L) conserving,
- R-parity conserving.

R-parity is needed to avoid a too rapid proton decay and is defined as $(-1)^{3\mathrm{B}+\mathrm{L}+2\mathrm{S}}$, where S denotes the Spin. Keeping in mind these assumptions, $\mathcal{L}_{\mathrm{SOFT}}$ contains the following terms:

$$\begin{aligned}
\mathcal{L}_{\mathrm{SOFT}} = &- m_{\tilde{q}}^2|\tilde{q}_L|^2 - m_{\tilde{u}}^2|\tilde{u}_R|^2 - m_{\tilde{d}}^2|\tilde{d}_R|^2 - m_{\tilde{l}}^2|\tilde{l}_L|^2 - m_{\tilde{e}}^2|\tilde{e}_R|^2 && (3.15)\\
&- \epsilon_{ij}(\lambda_u A_u H_2^i \tilde{q}_L^j \tilde{u}_R^\dagger + \lambda_d A_d H_1^i \tilde{q}_L^j \tilde{d}_R^\dagger + \lambda_e A_e H_1^i \tilde{l}_L^j \tilde{e}_R^\dagger + h.c.) && (3.16)\\
&- \epsilon_{ij}(m_3^2 H_1^i H_2^j + h.c.) - m_1^2|H_1|^2 - m_2^2|H_2|^2 && (3.17)\\
&+ \frac{1}{2}(M_1\lambda'\lambda' + M_2\lambda^a\lambda^a + M_3\lambda_s^a\lambda_s^a + h.c.) && (3.18)
\end{aligned}$$

as L. Girardello and M. T. Grisaru have shown in 1982 [30]. The first line describes the soft SUSY breaking masses, the second covers the trilinear couplings and the third includes the Higgs terms whereas the last line contains the ones for the gauginos.

3.3 Supersymmetry Breaking and Flavour violation

As mentioned above, the parameters of $\mathcal{L}_{\mathrm{SOFT}}$ are determined by the soft SUSY breaking mechanism. So if we are able to measure the parameters we can learn something about the breaking mechanism. This might be far in the future but a well motivated task to do, after non-minimal flavour violation within the MSSM has been verified. To make a step into this direction, we pay attention to the fact that the soft-susy-breaking terms contain parameters which have an impact on the masses and the mixing of squarks. The squark masses arise from the soft SUSY breaking potential, which is given for the squarks $\tilde{q}_L, \tilde{u}_R, \tilde{d}_R$:

$$\begin{aligned}
V_{SOFT}^{\tilde{q}} = &\tilde{q}_{\alpha L}^\dagger (m_{\tilde{q}}^2)_{\alpha\beta}\tilde{q}_{\beta L} + \tilde{u}_{\alpha R}^\dagger (m_{\tilde{u}}^2)_{\alpha\beta}\tilde{u}_{\beta R} + \tilde{d}_{\alpha R}^\dagger (m_{\tilde{d}}^2)_{\alpha\beta}\tilde{d}_{\beta R}\\
&+ [H_2\tilde{q}_{\alpha L}(f^u A^u)_{\alpha\beta}\tilde{u}_{\beta R}^* + H_1\tilde{q}_{\alpha L}(f^d A^d)_{\alpha\beta}\tilde{d}_{\beta R}^* + h.c.] && (3.19)
\end{aligned}$$

with the mass matrices $m \in \mathbb{C}^{3\times 3}$, therefore $\alpha, \beta = 1, 2, 3$, given in the CKM basis. H_1 and H_2 denote the Higgs doublets and f^u, f^d the Yukawa couplings.

Super CKM Basis

Studying flavour violation is easier in what is known as the super CKM basis (SCKM). It results by rotating the interaction basis with the unitary transformations $V_{L,R}^{u,d}$ forming the CKM matrix the same way as in the SM. The flavour conserving MSSM is characterised by diagonal mass matrices in Equations (3.22), (3.23), and (3.24). However, there is no reason why this should be the case in nature and leads, in addition to the CKM mixing, to a new source of flavour violation. Together with the potentials stemming from D- and F-terms, see [31] the Lagrangian will contain the term:

$$-\mathcal{L}_m^{\tilde{q}} = \sum_{\tilde{q}} \tilde{q}^\dagger \mathcal{M}_{\tilde{q}}^2 \tilde{q} \tag{3.20}$$

with the hermitian 6×6 matrix for either $u-$ or $d-$type squarks:

$$\mathcal{M}_{\tilde{q}}^2 = \begin{pmatrix} M_{\tilde{q}LL}^2 & (M_{\tilde{q}RL}^2)^\dagger \\ M_{\tilde{q}RL}^2 & M_{\tilde{q}RR}^2 \end{pmatrix} \tag{3.21}$$

and each entry consists in turn of a 3×3 submatrix and is given considering merely up-type quark flavour violation (UQFV):

$$(M_{\tilde{u}LL}^2)_{\alpha\beta} = m_{\tilde{q}\alpha\beta}^2 + [(\frac{1}{2} - \frac{2}{3}\sin^2(\theta_W))\cos(2\beta)m_Z^2 + m_{u_\alpha}^2]\delta_{\alpha\beta}, \tag{3.22}$$

$$(M_{\tilde{u}RR}^2)_{\alpha\beta} = m_{\tilde{u}\alpha\beta}^2 + [\frac{2}{3}\sin^2(\theta_W)\cos(2\beta)m_Z^2 + m_{u_\alpha}^2]\delta_{\alpha\beta}, \tag{3.23}$$

$$(M_{\tilde{u}RL}^2)_{\alpha\beta} = (\frac{v_2}{\sqrt{2}})A_{u\alpha\beta} - m_{u_\alpha}\mu^* \cot(\beta)\delta_{\alpha\beta}, \tag{3.24}$$

wherein θ_W denotes the weak mixing angle, m_Z the Z pole mass, $m_{u,d}$ the quark masses, $\tan\beta$ the ratio of the vacuum expectation values of the two Higgs doublets H_1, H_2 and μ the so-called $\mu-$parameter. In the following we will use e.g. "13" as short notation for mixing between the first and third generation. If $\mathcal{M}_{\tilde{q}}^2$ is hermitian, then the two blocks on the diagonal must be hermitian, too. We can either mix left- and right-handed states, or generations, or both. "LL" and "RR" entries of each generation can be influenced by the diagonal entries, precisely by $m_{\tilde{q}\alpha\alpha}$ and $m_{\tilde{u}\alpha\alpha}$ respectively, whereas "LL" and "RR" mixing among different generations is controlled via the off-diagonal entries $m_{\tilde{q}\alpha\beta}$ and $m_{\tilde{u}\alpha\beta}$ for $\alpha \neq \beta$. "LR" and "RL" mixing is governed by the two remaining off-diagonal blocks, in detail by $A_{u\alpha\beta}$. If $\alpha = \beta$ we have mixing within one and the same generation, whereas if $\alpha \neq \beta$ between generation α and β. As these are off-diagonal blocks, they must not be hermitian, but $M_{\tilde{u}RL\alpha\beta} = M_{\tilde{u}LR\beta\alpha}$ must hold. Note, that the submatrices $m_{\tilde{q}\alpha\beta}^2$, $m_{\tilde{u}\alpha\beta}^2$ and $A_{u\alpha\beta}$ are the ones of Equation (3.19) and will be our main input parameters.

Nevertheless we are still dealing with unphysical squark eigenstates and must rotate these to a physical mass basis. This can be achieved by introducing two complex 6×6 matrices, $R^{\tilde{u}}$ for the up- and $R^{\tilde{d}}$ for the down-sector.

$$\begin{pmatrix} \tilde{u}_1 \\ \tilde{u}_2 \\ \tilde{u}_3 \\ \tilde{u}_4 \\ \tilde{u}_5 \\ \tilde{u}_6 \end{pmatrix} = R^{\tilde{u}} \begin{pmatrix} \tilde{u}_L \\ \tilde{c}_L \\ \tilde{t}_L \\ \tilde{u}_R \\ \tilde{c}_R \\ \tilde{t}_R \end{pmatrix}. \tag{3.25}$$

These eigenstates are mass-ordered, i.e. $\tilde{u}_1 < ... < \tilde{u}_6$ and each $\tilde{u}_i$ is a mixture of the six up-type squarks $\tilde{u}_L, \tilde{c}_L, ..., \tilde{t}_R$. The whole procedure can be summarized by the following table:

basis	quarks	squarks
interaction	$\{u^o_{\alpha L,R}, d^o_{\alpha L,R}\}$	$\{\tilde{u}^o_{\alpha L,R}, \tilde{d}^o_{\alpha L,R}\}$
	$\downarrow V^{u,d}_{L,R}$	$\downarrow V^{u,d}_{L,R}$
SCKM	$\{u_{\alpha L,R}, d_{\alpha L,R}\}$	$\{\tilde{u}_{\alpha L,R}, \tilde{d}_{\alpha L,R}\}$
	$\downarrow \mathbb{1}$	$\downarrow R^{u,d}$
mass	$\{u_{\alpha L,R}, d_{\alpha L,R}\}$	$\{\tilde{u}_\gamma, \tilde{d}_\gamma\}$

Table 3.1: Procedure of transforming from the interaction basis to a physical basis within the NMFV MSSM.

Here, $\mathbb{1}$ denotes the identity matrix and the index γ runs from 1 to 6. Note that in the MSSM without extra flavour violation the last step is not necessary because the mass matrices already are diagonal.

Flavour violating Parameters

To study QFV it is convenient to define some dimensionless parameters:

$$\delta^{uLL}_{\alpha\beta} := \frac{m^2_{\tilde{q}\alpha\beta}}{\sqrt{m^2_{\tilde{q}\alpha\alpha} m^2_{\tilde{q}\beta\beta}}}, \tag{3.26}$$

$$\delta^{uRR}_{\alpha\beta} := \frac{m^2_{\tilde{u}\alpha\beta}}{\sqrt{m^2_{\tilde{u}\alpha\alpha} m^2_{\tilde{u}\beta\beta}}}, \tag{3.27}$$

$$\delta^{uRL}_{\alpha\beta} := \frac{v_2}{\sqrt{2}} \cdot \frac{A_{u\alpha\beta}}{\sqrt{m^2_{\tilde{u}\alpha\alpha} m^2_{\tilde{q}\beta\beta}}}, \tag{3.28}$$

which vary between $[-1, 1]$ and avoid negative mass eigenvalues during the diagonalisation procedure to gain the squark masses. We perform the variation of these parameters with the public code SPheno, version 3.0.beta56 [32]. Consistent to this, we use the program to check the results with experimental constraints from B-Physics, as well as current LHC exclusion limits and vacuum stability conditions. The latter restrict "RL" and "LR" mixing, whereas flavour changing neutral currents (FCNC) processes limit generation mixing, as we will see in the next Chapter.

CHAPTER 4

Experimental and theoretical Constraints

Despite the fact that we do not yet know whether SUSY is realized in nature, measurements of certain observables, especially from electroweak and $B-$Physics can limit the parameters δ_{13}^{uRR} and δ_{13}^{uLR}, which drive the production of the final partonic state $2b + 2l^{+} + E_T^{miss}$. In this Chapter we will study experimental and theoretical constraints. The electroweak $\rho-$parameter has been measured very precisely, so corrections containing supersymmetric particles are bounded. However, δ_{13}^{uLR} can also be constrained by vacuum stability conditions [41]. At last we take recent exclusion limits on the squark and gluino masses from the LHC into account. We want to make a sensible analysis for one set of parameters. This has to fulfill the following constraints to make sure that it has not been excluded by now.

4.1 $B-$Physics Observables

In $B-$Physics flavour changing neutral current (FCNC) processes are very sensitive to new physics, because they have no Standard Model contributions at tree level. So the leading order contributions, here at the one-loop level may, already, contain supersymmetric particles. They can be calculated by using an effective low energy theory approach, where heavy particles are, basically, removed from the theory. This method goes back to Enrico Fermi, who used this procedure to describe weak interactions mediated via W bosons, which were still not discovered in the 1930's [33]. The idea is to use the so-called operator product expansion (OPE) and decompose the Hamiltonian:

$$H_{eff} \propto \sum_i [C_i(\mu) O_i + C_i'(\mu) O_i']. \tag{4.1}$$

The operators O_i are model-independent and non-perturbative. Therefore, the matrix elements must be evaluated at a low energy scale, e.g. $\mu = m_Z$. The primed operators are given by exchanging $L \leftrightarrow R$, these are important within NMFV, e.g. the so-called gluonic dipole operator $O_8' = g_s/(16\pi^2) m_b (\bar{d}_R \sigma^{\mu\nu} T^a b_L) G^a_{\mu\nu}$. All effective Hamiltonians are given in [34]. The Wilson coefficients $C_i(\mu)$ are model-dependent and calculable by using perturbative methods which are implemented e.g. in FeynArts [36]. They contain all the information about the considered model, which in our case is the MSSM and its flavour violating parameters. After these have been calculated one can perform the running down to the appropriate scale $\mu = m_b$ by making use of the renormalisation group equations (RGE) for the Wilson coefficients:

$$\mu \frac{d}{d\mu} C_i(\mu) = \hat{\gamma}^T(\mu) C_i(\mu), \tag{4.2}$$

with the anomalous dimension matrix:

$$\hat{\gamma}^T(\mu) = \sum_{n,m \geq 0} \hat{\gamma}^{(nm)} \tilde{\alpha}_s(\mu)^n \tilde{\alpha}_e(\mu)^m, \tag{4.3}$$

which contains the running of the electroweak $\tilde{\alpha}_e(\mu)$ and strong couplings $\tilde{\alpha}_s(\mu)$, where $\tilde{\alpha} = \alpha/4\pi$ and n, m denote the loop orders

$$\mu \frac{d\tilde{\alpha}_{s/e}}{d\mu} = \mp \tilde{\alpha}^2_{s/e} \sum_{n,m \geq 0} \beta^{s/e}_{nm} \tilde{\alpha}^n_{s/e} \tilde{\alpha}^m_{e/s}. \tag{4.4}$$

This relation, the beta functions $\beta^{s/e}_{nm}$ and more details can be found in [37]. The calculation of the following processes can be performed as explained and are automated by SPheno [32].

The following two tables show established low energy observables for ”23” and ”13” mixing, respectively. Compared to upper bounds, the measured observables with a central value serve as stringent constraints. The values have been taken from the Heavy Flavor Averaging Group [38].

	mixing between generation 2 and 3		
observable	$BR(B_s \to X_s\gamma)$	$BR(B_s \to \mu^+\mu^-)$	$\|\Delta M_{B_s}\|$
measured value	$(3.55 \pm 0.24 \pm 0.09) \cdot 10^{-4}$	$< 2.0 \cdot 10^{-7}$	$17.77 \pm 0.10 \pm 0.07$ ps^{-1}

Table 4.1: Low energy observables containing ”23” mixing and their measured value.

	mixing between generation 1 and 3		
observable	$BR(B_d \to \rho^0\gamma)$	$BR(B_d \to \mu^+\mu^-)$	$\|\Delta M_{B_d}\|$
measured value	$0.86^{+0.15}_{-0.14} \cdot 10^{-6}$	$< 5.1 \cdot 10^{-8}$	0.507 ± 0.004 ps^{-1}

Table 4.2: Low energy observables containing ”13” mixing and their measured value.

For the transitions we consider the branching ratios $BR(B_s \to X_s\gamma)$, $BR(B_d \to \rho^0\gamma)$, $BR(B_s \to \mu^+\mu^-)$ and $BR(B_d \to \mu^+\mu^-)$. The mass differences ΔM_{B_s} and ΔM_{B_d} result from $B\bar{B}-$oscillations. All of these observables can be calculated with SPheno [32] but $b \to d\gamma$ afforded some small modifications in the code.

Radiative Transitions

The radiative transitions $b \to s\gamma$ and $b \to d\gamma$ are initiated at the one loop level and characterised by emitting a photon, e.g. one possible contribution is Figure 4.1:

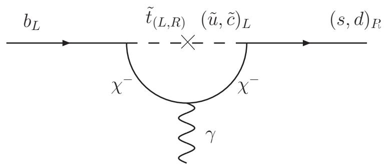

Figure 4.1: Chargino contribution to $b \to (s,d)\gamma$.

The charginos χ^- being a mixture of bino, wino and higgsinos couple to a left- and a right-handed squark. Hence, we can have "LR" mixing besides "32" and "31" generation mixing.

Starting point is the effective Hamiltonian [2]:

$$H_{eff} = -\frac{4G_F}{\sqrt{2}} V_{ts}^* V_{tb} \sum_{i=1}^{8} (C_i(\mu) O_i + C_i'(\mu) O_i'). \tag{4.5}$$

It leads to the decay width of $B_s \to X_s\gamma$ and $B_d \to \rho^0\gamma$, which have a similar structure:

$$\Gamma(B_s \to X_s\gamma) = \frac{m_b^5 G_F^2 \alpha_e}{32\pi^4} |V_{ts}^* V_{tb}|^2 K_{LO}, \tag{4.6}$$

$$\Gamma(B_d \to \rho^0\gamma) = \frac{G_F^2 \alpha_e}{32\pi^4} \left(1 - \frac{m_{\rho_0}^2}{m_B^2}\right)^3 |V_{td}^* V_{tb}|^2 m_B^3 m_b^2 K_{LO} \cdot 4.21 \cdot 10^{-2}, \tag{4.7}$$

where K_{LO} contains the relevant Wilson coefficients, see [2]. The branching ratios can be calculated via the decay width and the branching ratio of the process $B \to X_c e\bar{\nu}$:

$$\Gamma(B \to X_c e\bar{\nu}) = \frac{G_F^2 m_b^5}{192\pi^3} f(z)|V_{cb}|^2 \quad \text{and} \quad BR(B \to X_c e\bar{\nu}) \approx 0.106, \tag{4.8}$$

with $f(z) = 1 - 8z(1-z^2) - z^4 - 12z^2 \ln z$ and $z = (m_c/m_b)^2$. Inserting these expressions leads to:

$$BR(B_s \to X_s\gamma) = \frac{\Gamma(B_s \to X_s\gamma)}{\Gamma(B \to X_c e\bar{\nu})} \cdot BR(B \to X_c e\bar{\nu}) \tag{4.9}$$

$$= \frac{6\alpha_e}{\pi f(z)} \left| \frac{V_{ts}^* V_{tb}}{V_{cb}} \right|^2 K_{LO} \cdot 0.106 \tag{4.10}$$

$$BR(B_d \to \rho^0\gamma) = \frac{\Gamma(B_d \to \rho^0\gamma)}{\Gamma(B \to X_c e\bar{\nu})} \cdot BR(B \to X_c e\bar{\nu}) \tag{4.11}$$

$$= \frac{6\alpha_e\left(1 - \frac{m_{\rho_0}^2}{m_B^2}\right)^3 m_B^3 \cdot 4.21 \cdot 10^{-2}}{\pi m_b^3 f(z)} \left| \frac{V_{td}^* V_{tb}}{V_{cb}} \right|^2 K_{LO} \cdot 0.106. \tag{4.12}$$

So basically they just differ by a prefactor and the Wilson coefficients. The possibility of switching from s to d within the SPheno code was already implemented and mandatory for K_{LO}. We simply had to adjust the prefactor.

Semileptonic Transitions

Besides radiative decays semileptonic ones can also be taken as constraints. Often, e.g. [3] and [2], the process $B \to X_{s,d} l^+ l^-$, Figure 4.2 is used, which is quite similar to $b \to (s,d)\gamma$ and mainly serves as a constraint for "LL" mixing. We do not consider "LL" mixing and therefore, it can be neglected for same-sign top production.

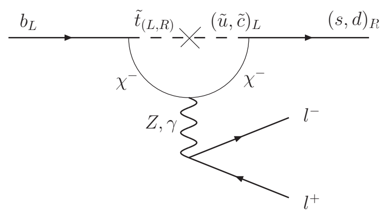

Figure 4.2: A flavour violating contribution to $B \to X_{s,d} l^+ l^-$.

Instead we use $B_{d,s} \to \mu^+\mu^-$. The effective Hamiltonian [35] reads:

$$H_{eff} = -\frac{4G_F}{\sqrt{2}\pi} V_{td}^* V_{tb} \sum_{i=10,S,P} (C_i(\mu)O_i + C_i'(\mu)O_i'), \tag{4.13}$$

S and P denote scalar and pseudo scalar operators, which differ by γ_5. It leads to the branching ratio:

$$BR(B_d \to \mu^+\mu^-) = \frac{G_F^2 \alpha_e^2 m_{B_d}^2 f_{B_d}^2 \tau_{B_d}}{64\pi^3} |V_{td}^* V_{tb}|^2 K_{LO}, \tag{4.14}$$

with the decay constant f_{B_d} from lattice theory and the lifetime τ_{B_d}. For K_{LO} we refer to [35]. It is obtained analogously to the strange quark version. This rate was already implemented in SPheno.

$B - \bar{B}$ Oscillations

In addition we used the mass differences $|\Delta M_{B_s}|$ and $|\Delta M_{B_d}|$. Analogously to kaon mixing the B_s^0 meson can oscillate into a $\bar{B}_s^0$ meson due to electroweak interactions, as shown in Figure 4.3:

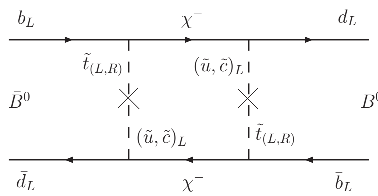

Figure 4.3: NMFV chargino contribution to $B - \bar{B}$ oscillations.

The mass difference can be obtained from the squared matrix element:

$$\Delta M_{B_s} = 2|\langle \bar{B}|H_{eff}|B\rangle|^2, \tag{4.15}$$

with [2, 34]:

$$H_{eff} = \frac{G_F^2 M_W^2}{16\pi^2} (V_{tb}^* V_{td})^2 \Big(\sum_{i=1}^{5} C_i(\mu)O_i + \sum_{i=1}^{3} C_i'(\mu)O_i' + h.c. \Big). \tag{4.16}$$

Again, we can read off the diagram in Figure 4.3 that ”RR” mixing will hardly effect this process. It is reasonable that these processes constrain down-type stronger than up-type NMFV. As we only focus on up-type QFV the constraints will not be as important as in studies of e.g. δ_{13}^{dLR}. Hence, larger values and therefore mixings can still be achieved, even around $\delta^u \approx 0.5$. In general, we can conclude that ”LR 13” mixing and ”RR 13” mixing mostly affects radiative decays and $B - \bar{B}$ oscillations, but far less than ”LL” mixing would do. These results will be included in Chapter 5.

4.2 Electroweak $\rho-$Parameter

The electroweak $\rho-$parameter was defined by D.A. Ross and M. Veltman in 1975 [39] as β, which is given by the ratio of the neutral and charged currents:

$$\beta := \frac{J_{NC}(0)}{J_{CC}(0)} = \frac{M_W^2}{M_Z^2 \cos\theta_W} =: \rho \tag{4.17}$$

The neutral current J_{NC} is extracted from the muon decay and the charged current J_{CC} from neutrino scattering at zero momentum transfer. With regards to the definition of the Weinberg angle $\cos\theta_W = \frac{g_2}{\sqrt{g_1^2+g_2^2}} = \frac{M_W}{M_Z}$, ρ is equal to 1 at LO. The quantum corrections to this parameter are given by [40]:

$$\Delta\rho = \mathrm{Re}\Big(\frac{\Sigma_Z^T(0)}{M_Z^2} - \frac{\Sigma_W^T(0)}{M_W^2}\Big) \tag{4.18}$$

where $\Sigma^T(0)$ denotes the transverse[1] part of the unrenormalised W and Z boson selfenergies. As a loop correction, it can include SUSY particles and therefore, information about non-minimal flavour violation. The $\rho-$parameter has been measured quite precisely [38] and its deviation from one should be less than 0.0012, which means:

$$\Delta\rho < 0.0012. \tag{4.19}$$

This serves as additional constraint when we are choosing the NMFV parameters.

4.3 Vacuum Stability Conditions

Far more important constraints concerning "LR" mixing induced by the trilinear coupling matrix, are the vacuum stability conditions [41]:

$$|T_{u\alpha\alpha}|^2 < 3f^{u_\alpha}(M^2_{Q\alpha\alpha} + M^2_{u\alpha\alpha} + (m^2_{H^\pm} + m_Z^2 \sin\theta_W)\sin^2\beta - \frac{1}{2}m_Z^2), \tag{4.20}$$

$$|T_{u\alpha\beta}|^2 < 3f^{u_\gamma}(M^2_{Q\alpha\alpha} + M^2_{u\beta\beta} + (m^2_{H^\pm} + m_Z^2 \sin\theta_W)\cos^2\beta - \frac{1}{2}m_Z^2), \tag{4.21}$$

where $\gamma = \max_{\alpha\neq\beta}(\alpha, \beta)$. These assure the minima of the superpotential, Equation (3.19) not to break charge and colour (CCB) symmetry. This is highly recommended for our work.

4.4 LHC Exclusion Limits

Squarks

At last our attention is drawn to recent exclusion limits from ATLAS [44] and CMS [45] to construct a squark mass spectrum. Because the analyses have been made for simplified SUSY scenarios, we take a more conservative bound concerning the masses. As Figures 4.4 and 4.5 show, basically no discovery channel has excluded squark masses above 1 TeV.

[1] which means that the application of its projector vanishes, $(k^2 g^{\mu\nu} - k^\mu k^\nu)\Sigma^T_{\mu\nu} = 0$.

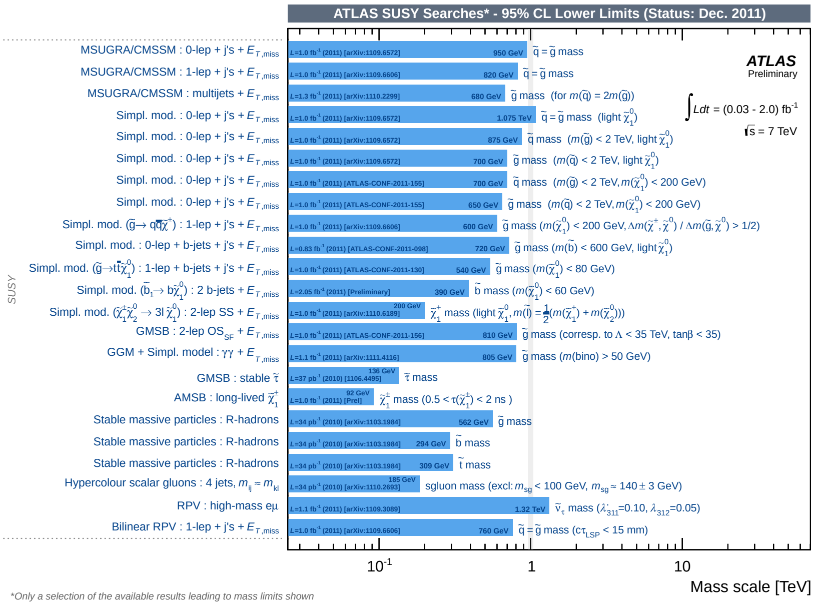

Figure 4.4: A combination of different analyses performed by the ATLAS collaboration.

These plots are obtained upon the assumption of averaged squark masses and therefore, we consider the average to be less than 1 TeV:

$$\bar{m}_{\tilde{q}} = \frac{m_{\tilde{u}1} + m_{\tilde{u}2} + m_{\tilde{u}3} + m_{\tilde{u}4} + m_{\tilde{u}5} + m_{\tilde{u}6}}{6} \leqq 1 \text{ TeV} \tag{4.22}$$

Roughly, the size of the squark masses is given by the diagonal entries of the four blocks in the mixing matrix:

$$\mathcal{M}^2_{\tilde{q}} = \begin{pmatrix} M^2_{\tilde{q}LL} & (M^2_{\tilde{q}RL})^\dagger \\ M^2_{\tilde{q}RL} & M^2_{\tilde{q}RR} \end{pmatrix} \tag{4.23}$$

which are built up according to Chapter 3.3 explicitely by:

- in the "LL" Block: $m^2_{\tilde{q}11}$, $m^2_{\tilde{q}22}$, $m^2_{\tilde{q}33}$,
- in the "RR" Block: $m^2_{\tilde{u}11}$, $m^2_{\tilde{u}22}$, $m^2_{\tilde{u}33}$,
- in the offdiagonal "RL" and "LR" Blocks: A_{u11}, A_{u22}, A_{u33}.

In SPheno they correspond to the diagonal entries of BLOCK MSQ2, BLOCK MSU2 and BLOCK TU and are compatible with the conventions of the SUSY Les Houches Accord [47], [48]. Besides the squark masses we are also able to choose a gluino mass of 2 TeV.

Higgs

More recently, both big LHC experiments have seen an excess of events, probably due to Higgs production. Within two to three standard deviations σ, Higgs masses around 125 GeV can not be excluded at the 95% confindence level, see Figure 4.6 by the CMS Collaboration [43].

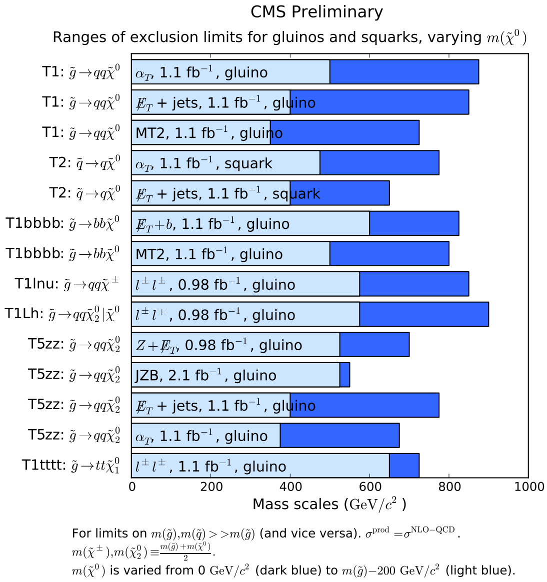

Figure 4.5: A combination of different analyses performed by the CMS collaboration.

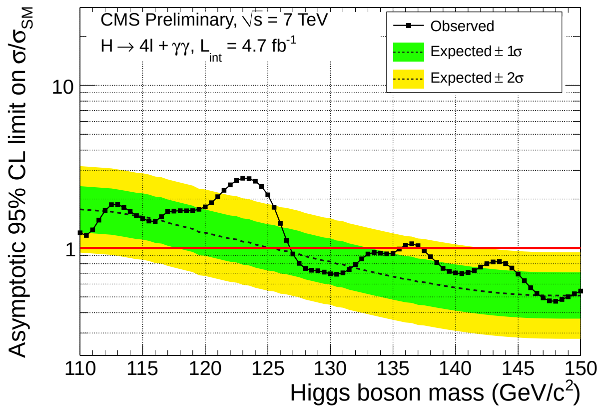

Figure 4.6: Most recent analysis of the two channels $H \to \gamma\gamma$ and $H \to 4l$ showing a peak slightly below 125 GeV. As it is an exclusion plot, a SM-type Higgs can not be excluded at the 95% CL.

However, it is too early to take a Higgs mass as a constraint into account, because it definitely has not yet been discovered. Anyway, the following work has been done before these results were published. The value for the SM like light Higss m_h calculated by SPheno in scenario (B), see Chapter 5.3, is 124.9 GeV.

Searches for same-sign leptons, b-tagged jets and missing energy

In march 2012 some results concerning the search of SUSY in events with same-sign leptons, bottom jets and missing energy have been published [46]. They considered two types of models. One was gluino pair production as shown in Figure 4.7 and the other was sbottom pair production, see Figure 4.8.

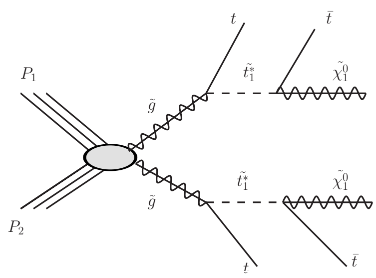

Figure 4.7: $pp \to tt\bar{t}\bar{t}$.

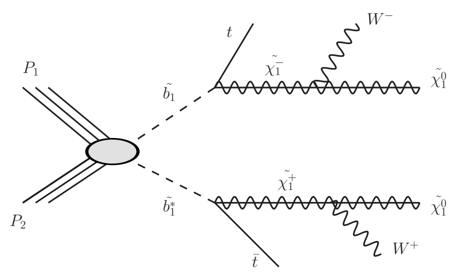

Figure 4.8: $pp \to t\bar{t}W^-W^+$.

At the moment, theire exists no official publication, explaining the details of these models. This makes it difficult to compare the results to the ones of our model. Using the data of 4.7 fb^{-1} integrated luminosity, they could make the following exclusions:

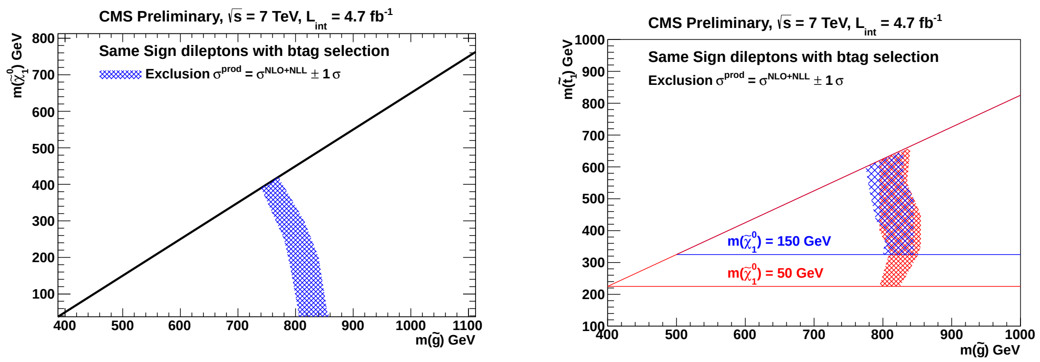

Figure 4.9: Exclusion plots from gluino pair production.

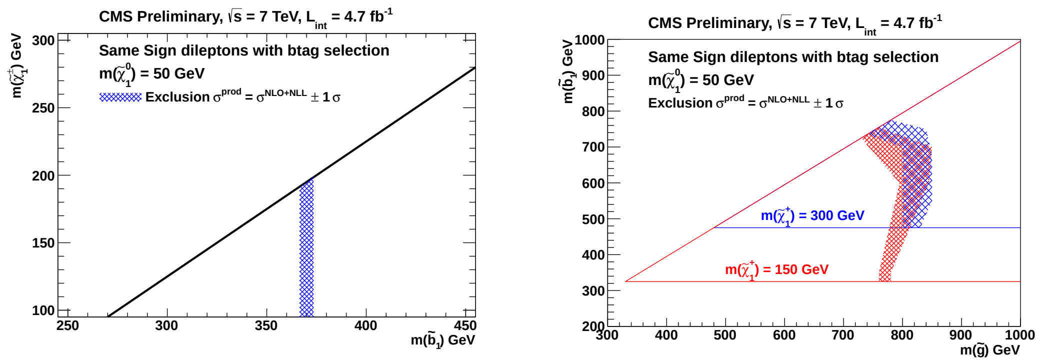

Figure 4.10: Exclusion plots from sbottom pair production.

The plots show only small areas which could be excluded. They do not overlap our sparticle mass regions, with gluinos of 2 TeV, neutralinos of 138 GeV and sbottoms of ≈ 1 TeV.

Summary

All listed constraints have been implemented in a C++ program, to perform an automatic check for a large number of values of δ_{13}^{uRR} and δ_{13}^{uLR}. To summarise, the strongest constraint is the electroweak $\rho-$parameter. The LHC exclusion limits have been appreciated in before hand and the diagonal values have not been tested to the extent of the off-diagonal ones. Nevertheless a check has been implemented. The vacuum stability conditions as well as the observables from $B-$Physics are hardly affected for two reasons. First we are interested in ”13” mixing, which is not as bounded as ”23” mixing and secondly, our masses are, being around 1 TeV, quite heavy and the observables are supressed by the squark masses. In agreement with the prediction in [41], ”LR” mixing is more strongly constrained by the vacuum stability conditions than ”RR” mixing by $B-$Physics. The results will be presented in Chapter 5.

CHAPTER 5

Signal Process

In this Chapter we will study the signal process, depicted in Figure 5.1, and explore how it is determined by NMFV. We will discuss different scenarios concerning light (A), medium (B) and very heavy squark masses (C). In scenario (A) we take values from [3] as a starting point, but consider "13" instead of "23" mixing. The (C) scenario is due to effective SUSY, see e.g. [51]. It is characterised by third generation squark masses of $\mathcal{O}(1\text{ TeV})$, whereas the ones of the first two generations are of $\mathcal{O}(10\text{ TeV})$[1]. The scenario (B) is chosen as the most ideal at the present time and provides us a benchmark point for the analysis in Chapter 6.

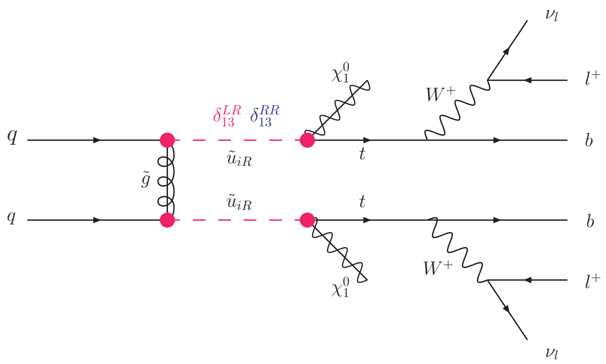

Figure 5.1: Same-sign top quark production via flavour violating t-channel gluino exchange.

Two quarks exchange a gluino in the t-channel and thereby turn into two squarks. Each, we require to decay into a top quark t and the stable neutralino χ_1^0. The top quarks decay into bottom quarks b and W^+ bosons. The latter again decays into a positively charged lepton l^+ and a neutrino ν_l. Flavour violation is possible at the pink highlighted regions. The squark starts in a flavour eigenstate at the first vertex and will mix during its propagation as a squark mass eigenstate until the next vertex, where it interacts as flavour eigentstate

[1] The detailed mass spectra will be presented later.

again. The squark eigenstate should be up-type and therefore is made up out of different percentages of $\tilde{u}_L, \tilde{c}_L, \tilde{t}_L, \tilde{u}_R, \tilde{c}_R, \tilde{t}_R$, preferably top squark. The relevant Feynman rules are as follows [31]:

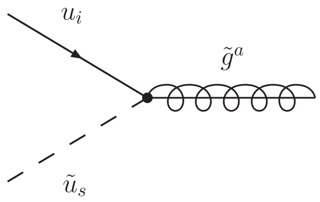

$$\Gamma_{u\tilde{u}\tilde{g}} = -i\sqrt{2} g_s T^a \sum_{j=1}^{3} (U_{ji}^{u_L} R_{js}^{\tilde{u}} P_R - U_{ji}^{u_R *} R_{j+3,s}^{\tilde{u}} P_L)$$

Figure 5.2: Quark-squark-gluino vertex.

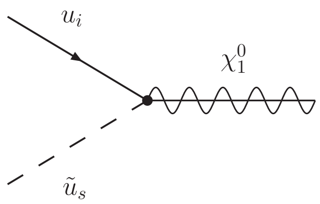

Figure 5.3: Quark-squark-neutralino vertex.

$$\begin{aligned}\Gamma_{u\tilde{u}\chi_1^0} = i\big[&[-\sqrt{2} g_s (\frac{1}{2} Z_{l2}^* + \frac{1}{6} \tan\theta_W Z_{l1}^*) \sum_{j=1}^{3} R_{js}^{\tilde{u}*} U_{ji}^{u_L} \\ &- \frac{g_2}{\sqrt{2} M_W \sin\beta} m_{u_i} Z_{l4}^* \sum_{j=1}^{3} R_{j+3,s}^{\tilde{u}*} U_{ji}^{u_R}]^* P_R \\ &+ [\frac{2\sqrt{2}}{3} g_2 \tan\theta_W Z_{l1} \sum_{j=1}^{3} R_{j+3,s}^{\tilde{u}*} U_{ji}^{u_R} \\ &- \frac{g_2}{\sqrt{2} M_W \sin\beta} m_{u_i} Z_{l4} \sum_{j=1}^{3} R_{js}^{\tilde{u}*} U_{ji}^{u_L}]^* P_L\big]\end{aligned}$$

with $i = \{1, 2, 3\}$, $s = \{1, 2, ..., 6\}$, $l = \{1, 2, 3, 4\}$ and $\alpha = \{1, 2, ..., 8\}$. For simplicity, only the up-type Feynman rule is given. The matrices U are unitary matrices due to CKM mixing, Z is needed for neutralino mixing and R for squark mixing, as explained in Chapter 3.

Implementation in Herwig++

The program Herwig++ is a Monte Carlo event generator, written in C++ [52]. This allows for an object-oriented construction where all necessary modules can be arranged as classes. It includes the generation of matrix elements based on a certain model, e.g. the SM, MSSM, NMSSM, or ADD. After calculating the total cross section a parton shower, underlying event and hadronisation can be simulated. It is able to perform the generation of events up to the next-to-leading order (NLO) precision. For this purpose a matching procedure, either the MC@NLO [56] or POWHEG scheme [57], can be used to avoid double counting of real emissions. As we are interested in a parton level Monte Carlo analysis at leading order (LO), we can switch off these features and concentrate on the matrix elements.

Every vertex is described by a class. The mixing matrix is defined in a separate one. For our purpose we have enlarged the existing 2×2 stop (”stopmix”) and sbottom mixing matrices (”sbotmix”) to 6×6 dimensional matrices ”usqmix” and ”dsqmix”, respectively. They act as a pointer to the values given in the SPheno output file ”SPheno.spc”. We have modified the following classes and corresponding header files: ”MSSM.cc”, ”SusyBase.cc”, and all vertices containing a mixing matrix, especially the gluino-quark-squark vertex ”SSGFSVertex.cc” and the neutralino-quark-squark vertex ”SSNFSVertex.cc”. They are implemented according to the vertices of Figure 5.2 and 5.3. Every vertex containing a mixing matrix had to be changed to assure a smooth flow of the program and therefore, a consistent calculation.

Input Parameters

In the following we will study the NMFV parameters δ_{13}^{RR} and δ_{13}^{LR}. The inital state partons, in our case unpolarized quarks, can be left- as well as right-handed. The neutralino χ_1^0 is the lightest supersymmetric particle and therefore stable in our model. It is a mixture of bino, wino and higgsino. Whereas the wino only couples to left-handed particles, the bino, due to its hypercharge proportionality, couples to the right-handed particles. The χ_1^0, being the lightest neutralino, is mainly bino-like and therefore, the coupling to right-handed particles is enlarged. The higgsino part can be neglected, because it mainly contributes to the heavy neutralinos χ_3^0 and χ_4^0. We want the right-handed squark to decay into a neutralino χ_1^0 and a top quark. This can be achieved by inserting a "LR" and "RR" mixing from the first to the third generation at the two pink vertices in Figure 5.1. Hence, the propagating squark mass eigenstates are made up of as much right-handed top squark flavour as is still permitted by the constraints described in Chapter 4.

To generate a mass spectrum, many input parameters are used. Besides the CKM parameters mentioned in Chapter 2, the following SM (5.1) and Susy (5.2) parameters will be kept constant throughout all calculations.

$$1/\alpha_e^{\overline{MS}}(m_Z) = 127.9 \qquad \alpha_s^{\overline{MS}}(m_Z) = 0.119 \qquad v = 242 \text{ GeV} \tag{5.1}$$
$$m_Z^{pole} = 91.18 \text{ MeV} \qquad m_t^{pole} = 172.9 \text{ GeV}$$

$$M_1 = 139 \text{ GeV} \qquad M_2 = 500 \text{ GeV} \qquad M_3 = 2 \text{ TeV} \tag{5.2}$$
$$\mu = 1 \text{ TeV} \qquad \tan\beta = 10$$

Recently, the CMS experiment has performed an analysis of same-sign dilepton signals [58]. This can also be achieved in our process by leaving out the b-tagging and looking at the channel $2j + 2l^+ + E_T^{miss}$. For this reason we will have a look at the flavour conserving production of squarks before we concentrate on the flavour violating case.

5.1 Flavour conserving Production of Squarks

In the following section we will only focus on the production of top quarks within our signal process, which decay to taggable bottom quarks. However, this is not the only squark decay channel. The squark could decay into a W^- boson and a sbottom $\tilde{b}$ which in turn decays to bottom b and neutralino χ_1^0. This is only possible for left-handed squarks and suppressed according to the choice of our parameters for "RR" and "LR" mixing. Besides this, the squark could also decay into a chargino χ^+ and a bottom quark. Since it is the supersymmetric partner of the W^+ boson, the chargino χ^+ also only couples to left-handed squarks. Such production channels are incorporated in our background, see Chapter 6.

In general not only top quarks are produced. Light quarks, as d, u, s, c can also be produced. We will see later that by the use of b-tagging only certain percentages can be identified correctly and a small percentage will be mis-identified as a bottom quark. At high momentum transfer x the sea quark densities are much smaller and therefore, less likely to react in the hard process. In turn, this leads to hardly any bottom quarks but many light quarks in the final state.

Because the squarks in the signal process are scalar particles which decay in a cascade, the sum over spins and polarisations when we are calculating the cross section is trivial. The resonances of such heavy particles have a narrow width. Therefore, they are described very well by Breit-Wigner distributions and can be produced on-shell. Hence, the total cross section factorises,

$$\sigma(pp \to tt\chi_1^0\chi_1^0) = \sum_{i,j=1}^{6} \sigma(pp \to \tilde{u}_{iR}\tilde{u}_{jR}) \cdot BR(\tilde{u}_{iR} \to t\chi_1^0) \cdot BR(\tilde{u}_{jR} \to t\chi_1^0). \tag{5.3}$$

The squark production cross section $\sigma(pp \to \tilde{u}_{iR}\tilde{u}_{jR})$ is calculated by Herwig++ and the branching ratios by SPheno. We combine them in a C++ program, the same one, that checks the constraints. So first it inserts NMFV parameters, then checks the constraints and if these are fulfilled Herwig++ is executed. At last it puts everything together and writes the results to a file. The program can be visualised by the following flow chart.

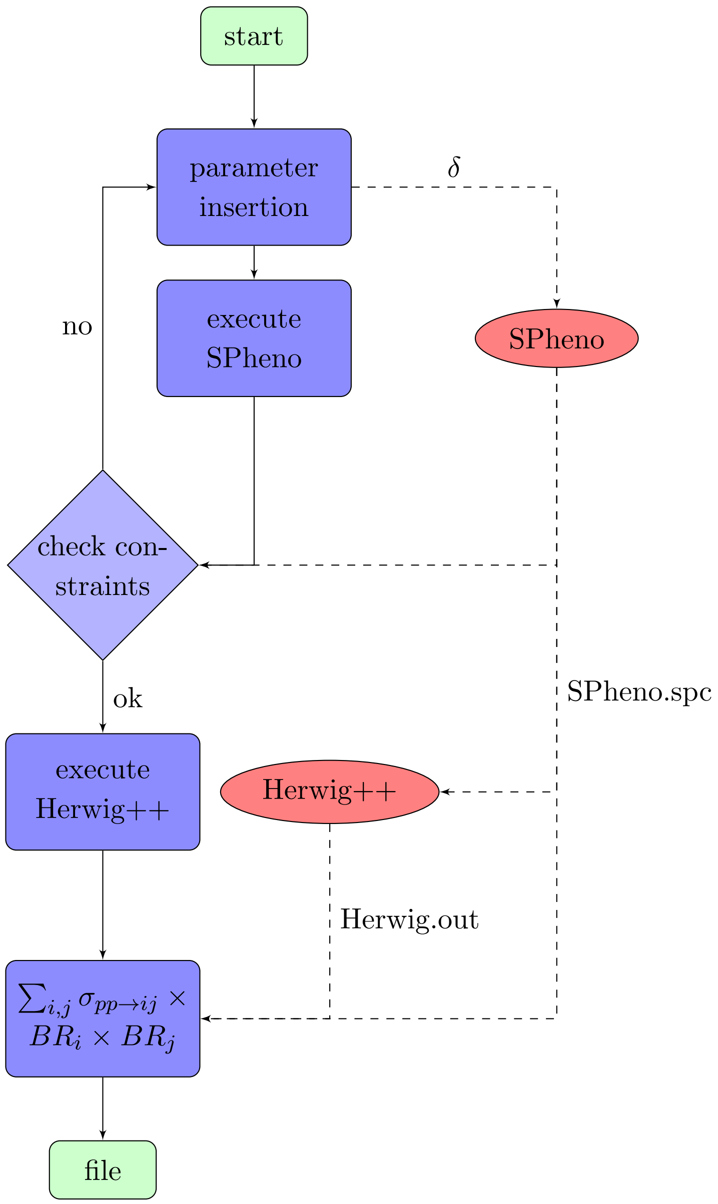

The red clouds show external programs, which can be executed by the main program, presented by blue blocks. The continuous lines correspond to the history of the program, the dashed lines to data which is passed to various procedures within the blue blocks.

Exemplary, by using the parameters given in Table 5.5 and setting the off-diagonal entries of the four blocks to zero, which corresponds to mixing between left and right handed states but not among generations, we obtain a total cross section of:

$$\begin{aligned}\sigma_{pp\to d^i d^j l^+ l^+ \chi_1^0\chi_1^0} &= \sum_{i,j=1}^{3} \sigma_{pp\to u^i u^j \chi_1^0\chi_1^0} \cdot BR^2(u^{(i,j)} \to d^{(i,j)} W^+) \cdot BR^2(W^+ \to l^+ \nu_l) \\ &= 5.08 \text{ fb} \cdot (0.99)^2 \cdot (0.22)^2 = 0.24 \text{ fb},\end{aligned} \tag{5.4}$$

where i, j denote generation indices. As we are concerned with the flavour conserving squark pair production, u^i and u^j are mostly up or charm quarks. Note, that due to the branching ratios of Equation (5.4) only 4.7% of the quark pair production cross section $\sigma_{pp\to u^i u^j \chi_1^0\chi_1^0}$ remains.

5.2 Starting Point Scenario: A

The first scenario we have considered is based on Table 1 by Porod et al. [3]. They focus on QFV leading to considerable rates of $pp \to c\bar{t}(t\bar{c}) + E^T_{miss} + X$ but merely take "23" mixing into account. It has been shown by studying Higgs production in [2] that "13" mixing is not as limited and therefore, sizable mixings are possible. Although same-sign top production was treated as negligable for "23" mixing in [3], we will take "13" mixing into account and probe it. The crucial part will be the tagging of the b quarks arising from the top quark decay, which sets it apart from the background. Details are presented in Chapter 6.

The aim of this work is to see, whether flavour violation can be observed during the first years of running the LHC. Therefore we try to find the mixing parameters which lead to the most significant signal. This can be achieved by optimising the total cross section σ of $pp \to tt\chi_1^0\chi_1^0$. For this purpose we vary the two most relevant mixing parameters δ_{13}^{uRR} and δ_{13}^{uLR} corresponding to the horizontal x and vertical y axis in Figure 5.4. The following Table 5.1 lists the input parameters, as well as x and y, which show the corresponding matrix entries.

A	11	12	13	21	22	23	31	32	33
$m^2_{\tilde{q}\alpha\beta}/(10^4\ \text{GeV}^2)$	85	-	-	-	77	-	-	-	70
$m^2_{\tilde{u}\alpha\beta}/(10^4\ \text{GeV}^2)$	67	-	x	-	36	-	x	-	34
$m^2_{\tilde{d}\alpha\beta}/(10^4\ \text{GeV}^2)$	69	-	-	-	67	-	-	-	66
$A_{u\alpha\beta}$/GeV	0.007	-	-	-	2.68	-	y	-	488

Table 5.1: Fixed and variable (x, y) entries of the soft-breaking mass matrices $m^2_{\tilde{q}}$, $m^2_{\tilde{u}}$, $m^2_{\tilde{d}}$ and trilinear coupling matrix A_u.

With these and the other input parameters, given in Equations (5.1) and (5.2), the squark mass spectrum and the mixing matrix R^u are generated by SPheno. We assume a center of mass energy of $\sqrt{s} = 14$ TeV and diagonal entries possessing a descending hierarchy. Then, by varying x and y we obtain the following plot:

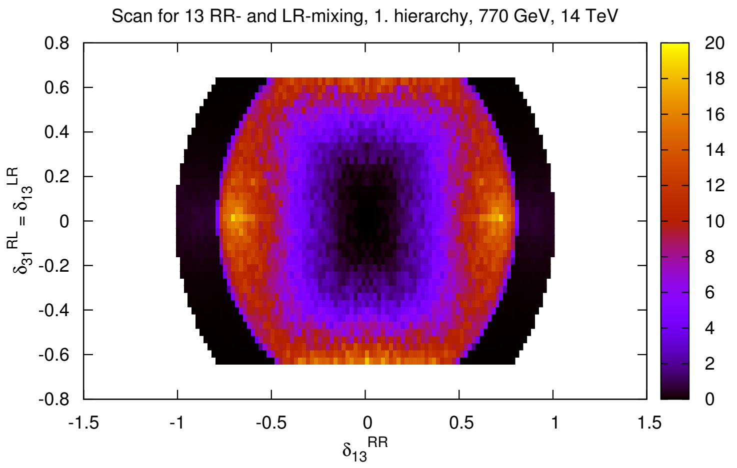

Figure 5.4: Total cross section in fb of same-sign top quark production $pp \to tt\chi_1^0\chi_1^0$ via flavour violating t-channel gluino exchange at $\sqrt{s} = 14$ TeV.

This shows the total cross section $\sigma^{tot}(pp \to tt\chi_1^0\chi_1^0)$ in fb. The white region corresponds to excluded parameters due to the constraints, mainly too small squark masses (<750 GeV in average) and vacuum stability conditions. The outer very dark to black region is due to a squark mass eigenstate which is so light that its decay into top quark and neutralino is kinematically forbidden. The inner dark region shows hardly any mixing so that the mass eigenstates do not contain any stop flavour and top quarks are not producible. At last, we can see four enhanced regions in orange to yellow. These are our maxima, where branching ratios and masses complement themselves, most ideal to gain a sizable total cross section. Exemplarily we choose the point $(m^2_{u13}/(10^4\ \text{GeV}^2)|A_{u13}/\text{GeV}) = (32|0)$ corresponding to $(\delta_{13}^{RR}|\delta_{13}^{LR}) = (0.67|0)$ which yields to the masses:

A	χ_1^0	χ_2^0	χ_1^+	$\tilde{g}$	$\tilde{u}_1$	$\tilde{u}_2$	$\tilde{u}_3$	$\tilde{u}_4$	$\tilde{u}_5$	$\tilde{u}_6$	$\bar{m}_{\tilde{u}}$
m/GeV	138	494	494	2000	391	599	817	849	920	944	753

Table 5.2: Neutralino, chargino, gluino and squark masses produced by input values in Table 5.1. The last column shows the averaged squark mass.

The lightest and therefore most abundant squark to produce is $\tilde{u}_1$. The first row of the mixing matrix R^u shows its composition of flavour eigenstates:

j	$\tilde{u}_L$	$\tilde{c}_L$	$\tilde{t}_L$	$\tilde{u}_R$	$\tilde{c}_R$	$\tilde{t}_R$
$(R^u_{1j})^2$	$1.05 \cdot 10^{-7}$	$0.79 \cdot 10^{-8}$	$2.16 \cdot 10^{-2}$	$2.71 \cdot 10^{-1}$	$5.10 \cdot 10^{-13}$	$7.07 \cdot 10^{-1}$

Table 5.3: First row of the mixing matrix $R^u(R^u)^T$. The values add up to 1.

Obviously $\tilde{u}_R$ and $\tilde{t}_R$ are the main parts as we would expect by choosing fairly sizable "RR 13" mixing. When we have a look at the branching ratios $\tilde{u}_i \to t\chi_1^0$:

i	1	2	3	4	5	6
$BR(\tilde{u}_i \to t\chi_1^0)$/GeV	58.68%	0%	0%	1.36%	0%	16.37%

Table 5.4: Branching ratios produced by input values in Table 5.1.

we can see that the decay of $\tilde{u}_1$ to t and χ_1^0 is the largest. In the end we can gain a total cross section of 17.5 fb. Note, the top quarks will decay further to bottom quarks and W^+ bosons, which again decay to l^+ and ν_l with a combined branching ratio of about 5%. Unfortunately, these squark masses are quite light and the exclusion limits have been raised by the LHC over the last few months. Hence, we have constructed a new scenario (B) with heavier squarks.

5.3 Threshold Scenarios: B

The second scenario we will discuss aims at squark masses of about 1 TeV, which are near the threshold of recent exclusion limits, presented in Chapter 4.4. At the same time they are far enough away not to be excluded during our calculations. Generally, the size is given by the diagonal entries of the mass matrix in Equation (3.21). In the following, we will consider a descending hierarchy on the one hand and on the other an ascending one. Neither experimental results, nor extrapolations of SUSY breaking at the GUT scale, provide a preference.

5.3.1 Hierarchy I

We have chosen the following diagonal values with descending hierarchy:

B	11	12	13	21	22	23	31	32	33
$m^2_{\tilde{q}\alpha\beta}/(10^4\ \mathrm{GeV}^2)$	111	-	-	-	103	-	-	-	96
$m^2_{\tilde{u}\alpha\beta}/(10^4\ \mathrm{GeV}^2)$	93	-	x	-	62	-	x	-	60
$m^2_{\tilde{d}\alpha\beta}/(10^4\ \mathrm{GeV}^2)$	222	-	-	-	222	-	-	-	222
$A_{u\alpha\beta}$/GeV	-0.021	-	-	-	-0.36	-	y	-	-34

Table 5.5: Fixed and variable (x, y) entries of the soft-breaking mass matrices $m^2_{\tilde{q}}$, $m^2_{\tilde{u}}$, $m^2_{\tilde{d}}$ and trilinear coupling matrix A_u, descending hierarchy.

After implementing them we varied again x and y and obtained the following plot showing the cross section $\sigma^{tot}(pp \to tt\chi_1^0\chi_1^0)$ in fb.

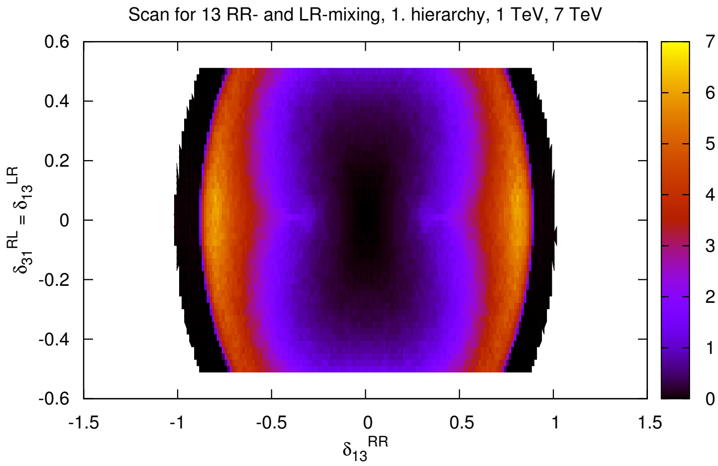

Figure 5.5: Total crossection in fb of same-sign top quark production $pp \to tt\chi_1^0\chi_1^0$ at $\sqrt{s} = 7$ TeV and $\int Ldt = 30$ fb^{-1}.

The visual motif is the same as in Figure 5.4. As the low energy observables are suppressed by the squark mass, the "RR" mixing is not as much constrained as in scenario (A). The vacuum stability conditions contain the squared mass matrix elements and therefore, there is a slightly stronger constraint to "LR" mixing in this scenario (B).

5.3.2 Hierarchy II

The next step is to reverse the hierarchy of the diagonal elements of $m^2_{\tilde{q}\alpha\beta}$ and $m^2_{\tilde{u}\alpha\beta}$ which form the diagonal of Equation (3.21).

B	11	12	13	21	22	23	31	32	33
$m^2_{\tilde{q}\alpha\beta}/(10^4\ \text{GeV}^2)$	60	-	-	-	62	-	-	-	93
$m^2_{\tilde{u}\alpha\beta}/(10^4\ \text{GeV}^2)$	96	-	x	-	103	-	x	-	111
$m^2_{\tilde{d}\alpha\beta}/(10^4\ \text{GeV}^2)$	222	-	-	-	222	-	-	-	222
$A_{u\alpha\beta}/\text{GeV}$	-0.021	-	-	-	-0.36	-	y	-	-34

Table 5.6: Fixed and variable (x, y) entries of the soft-breaking mass matrices $m^2_{\tilde{q}}$, $m^2_{\tilde{u}}$, $m^2_{\tilde{d}}$ and trilinear coupling matrix A_u, ascending hierarchy.

Again, x in terms of δ_{13}^{RR} is assigned to the horizontal and y is expressed through δ_{13}^{LR} on the vertical axis. We obtained the following plots at $\sqrt{s} = 7$ TeV (left) and $\sqrt{s} = 14$ TeV (right):

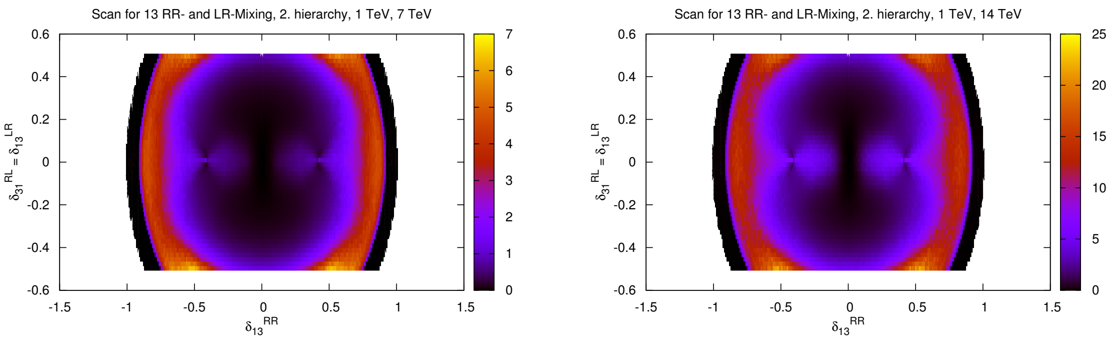

Figure 5.6: Total crossection in fb of same-sign top quark production $pp \to tt\chi_1^0\chi_1^0$, left at $\sqrt{s} = 7$ TeV and right at $\sqrt{s} = 14$ TeV.

In contrast to Figure 5.5 the visual motif changes a little. Of course, due to small mixings, we do not obtain sizable cross sections around (0|0). The dark area of small cross sections is larger than with a descending hierarchy. Besides this the maxima are located at the four corners instead of at the left and right edges. This is due to the fact that a descending hierarchy generates lighter $\tilde{u}_R$ than $\tilde{u}_L$, therefore, more "RR" mixing leads to an enhancement at the edges. Whereas an ascending hierarchy induces lighter $\tilde{u}_L$ and consequently maxima in the outer corners.

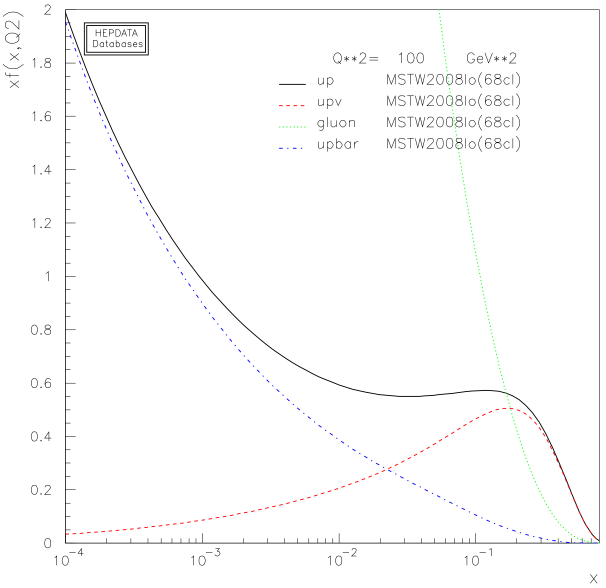

Figure 5.7: Parton densities.

The cross section rises by a factor of nearly four, going from $\sqrt{s} = 7$ TeV to $\sqrt{s} = 14$ TeV. This can be explained by the parton densities, cf. Figure 5.7, [59]. To produce two mass eigenstates of e.g. 400 GeV one needs a partonic center of mass energy $\hat{s}$ of at least 800 GeV. Assuming equal parts from both protons, a momentum fraction x of 0.11 at $\sqrt{s} = 7$ TeV or 0.06 at $\sqrt{s} = 14$ TeV is required. Both have the same value of $xu(x, Q^2) = 0.6$ for the up quark density (black line) and therefore we gain a factor four in the cross section, which is proportional to $u(x_1, Q^2)u(x_2, Q^2)$.

5.4 Scenarios with heavy Squarks: C

Recently the Atlas Collaboration presented an analysis searching for light third generation squarks and sleptons [61]. So far they have not seen any deviations of the SM with a luminosity of 2 fb^{-1}, resulting in some mass exclusion limits for light squarks, sleptons, gluinos and neutralinos. In this section we will explore a scenario with third generation squarks of about 1 TeV and the first and second of 15 TeV. Such a situation is known as effective Susy, see [51]. Possible parameters read:

C	11	12	13	21	22	23	31	32	33
$m^2_{\tilde{q}\alpha\beta}/(10^6\text{GeV}^2)$	230	-	-	-	230	-	-	-	1.7
$m^2_{\tilde{u}\alpha\beta}/(10^6\text{GeV}^2)$	230	-	-3.4	-	230	-	-3.4	-	1.7
$m^2_{\tilde{d}\alpha\beta}/(10^6\text{GeV}^2)$	230	-	-	-	230	-	-	-	1.7
$A_{u\alpha\beta}/(10^3\text{GeV})$	1	-	-	-	1	-	0	-	1

Table 5.7: Fixed entries of the soft-breaking mass matrices $m^2_{\tilde{q}}$, $m^2_{\tilde{u}}$, $m^2_{\tilde{d}}$ and trilinear coupling matrix A_u.

Within scenario (B) it is obvious that both hierarchies lead to sizable cross sections for large "RR" and vanishing "LR" mixing. This scenario (C) with $\delta_{13}^{RR} = 0.017$ is compatible with the constraints because, the low energy observables from $B-$Physics are supressed by the squark masses. The vacuum stability conditions only constrain "LR" mixing which is set to zero. Values larger than $\delta_{13}^{RR} = 0.017$ exceed the $\Delta\rho$ constraint. The exact squark masses are:

C	$\tilde{u}_1$	$\tilde{u}_2$	$\tilde{u}_3$	$\tilde{u}_4$	$\tilde{u}_5$	$\tilde{u}_6$	$\bar{m}_{\tilde{u}}$
m/TeV	1.23	1.38	15.16	15.16	15.17	15.17	10.55

Table 5.8: Squark masses produced by input values in Table 5.7. The last column shows the averaged squark mass.

These squark masses could only be achieved by a gluino mass of at least 2 TeV. Otherwise, a negative mass square, i.e. spontaneous colour breaking, is produced by the diagonalisation of the fermion masses which are calculated including higher order corrections in SPheno. Running the LHC at $\sqrt{s} = 14$ TeV produces only $\tilde{u}_1$ and $\tilde{u}_2$. The cross section obtained by Herwig++ reads:

$$\sigma_{pp\to\{\tilde{u}_1,\tilde{u}_2\}} = 0.71 \times 10^{-6} \text{ fb} \tag{5.5}$$

Bearing in mind that this has to be multiplied with the branching ratios of Equation (5.4); it is far too small to be measurable at the LHC. Actually, it is quite plausible, because the mixing compared to the other scenarios is very small. Therefore, the initial up quarks hardly mix a large part of top squark into mass eigenstates. Consequently, we will not study this case any further.

5.5 Benchmark Point

Now, after we have discussed several scenarios, but can only make an analysis per parameter set, we will choose a benchmark point. Obviously, the squark pair production cross section of scenario (C) is too small to lead to a viable analysis. Neither we will take parameters of scenario (A), because compared to scenario (B), 2nd hierarchy Figure 5.6 (right), the total cross section is smaller. Looking at scenario (B), we have studied two different hierarchies which lead to the same size of cross sections. It is sufficient to choose one parameter set. By comparing the shapes it makes sense to choose one out of the 1st hierarchy, Figure 5.5. The dark area in the middle is a bit smaller. Excessive constraints would bound our parameter space from the outside. For a future analysis, taking smaller parameters into account, this is slightly more promising. Now we are left with two equal maxima. Eventually, we choose:

$$(\delta_{13}^{RR}|\delta_{13}^{LR}) = (0.803|0.055). \tag{5.6}$$

These values corresponds to the entries $m_{\tilde{u}^2_{13}} = 60 \cdot 10^4$ GeV^2 and $A_{u31} = 300$ GeV in the squark mass matrix, Equations (3.23), (3.24). They lead to the following squark masses, Table 5.9 and a cross section of:

B	χ_1^0	χ_2^0	χ_1^+	$\tilde{g}$	$\tilde{u}_1$	$\tilde{u}_2$	$\tilde{u}_3$	$\tilde{u}_4$	$\tilde{u}_5$	$\tilde{u}_6$	$\bar{m}_{\tilde{u}}$
m/GeV	138	494	494	2000	398	787	993	1013	1051	1184	904

Table 5.9: Neutralino, chargino, gluino and squark masses produced by input values in Table 5.5 and Equation (5.6). The last column shows the averaged squark mass.

$$\sigma(pp \to tt\chi_1^0\chi_1^0) = 6.23 \text{ fb}. \tag{5.7}$$

CHAPTER 6

Prospects for the LHC

At the end of the previous Chapter we have chosen a benchmark point to perform a Monte Carlo based analysis. This will be addressed in the current Chapter. We want to find out, whether the signal gained by our benchmark point and containing $2b + 2l^+ + E^T_{miss}$ as final state is measurable at the LHC. This is the aim of our work. We explicitly state, that our analysis will be quite conservative and new, not yet well-established suggestions, leave potential for further improvements. If supersymmetry is really able to describe nature, this process could be used to probe flavour violation, especially between the first and third generation. Mixing of the second and third generation has already been discussed in [3], but so far no Monte Carlo study has been presented. In Chapter 5 we found a signal cross section of $\sigma(pp \to tt\chi^0_1\chi^0_1) = 6.23$ fb. If we want to see the flavour-violating signal, it has to be larger than the errors on the background. So the next step is to explore other processes with the same visible final state particles, which form the background.

6.1 Background Processes

The background processes can be divided into ones stemming from the Standard Model and others from supersymmetry. The general procedure is the following: Basically, we have to start with the partons of the proton and end at exactly:

- either two quark jets j, identified as b by mis-tagging,
- or two bottom quarks b,
- or a combination of a mis-identified quark j and a bottom jet b,

plus two same-sign leptons l^+. These particles are visible in the detector. Additionally, arbitrarily many merely weakly interacting particles, i.e. neutrinos ν and stable neutralinos χ^0_1, can be produced. They all form the missing transverse energy E^T_{miss}. In between, we include all possible transitions. This information regarding the initial requirements can be built into the input file of Herwig++. The final requirements are implemented in a two step analysis with ROOT [54]. The first step makes a rough selection of the final state particles during the run of Herwig++ and the second contains b-tagging efficiencies, cuts and fills histograms.

Backgrounds involving SUSY Particles

When we think of background processes within supersymmetry, we assume the $\mathcal{O}(\alpha_s^2\alpha^2)$ up-type QFV squark pair production and decay. Up- and anti-down-type squarks can be produced as intermediate states, whereas down- and anti-up-type ones are irrelevant for our analysis because they would lead to negatively charged leptons. As positively and negatively charged leptons are free elementary particles, they can be measured by the tracker and the electromagnetic calorimeter. Muons do not shower and therefore are detected in the outer muon chambers. We will not take hadronic tau decays into account, because they are identified by the hadronic calorimeter and form a different final state. Due to mis-identifications, we basically have the two types:

a) $pp \to jbl^+l^+$ and E^T_{miss}

b) $pp \to jjl^+l^+$ and E^T_{miss}

In the case of a) one b quark is produced analogously to the signal and the jet j is a lighter quark, which e.g. was produced via charginos as depicted in Figure 6.1:

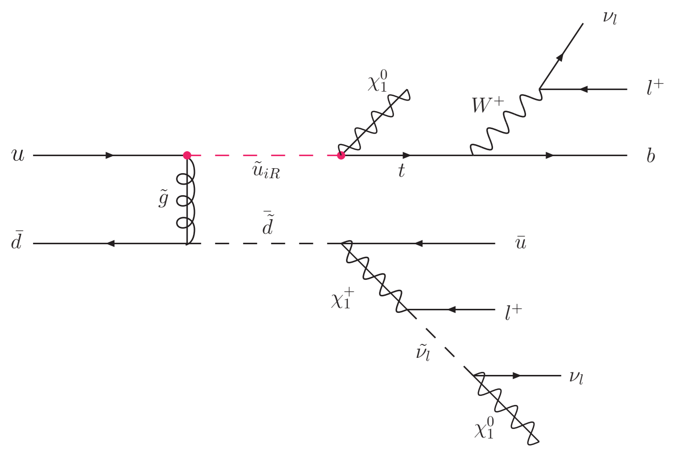

Figure 6.1: An example diagram of type a), in this case $\bar{u} \in \{\bar{u}, \bar{c}\}$ is the light jet.

The vertices and propagators involving QFV are highlighted. The final state light quark, despite the fact that it is up-type, may be mis-identified as a bottom quark. At the moment the distinction between particle and anti-particle, as well as the tagging of all quarks lighter than b quarks, is not advanced enough to be incorporated in a theory-based analysis. But we will keep this possibility in mind for the future. The same can happen to both quark jets in the case of b) in Figure 6.2,

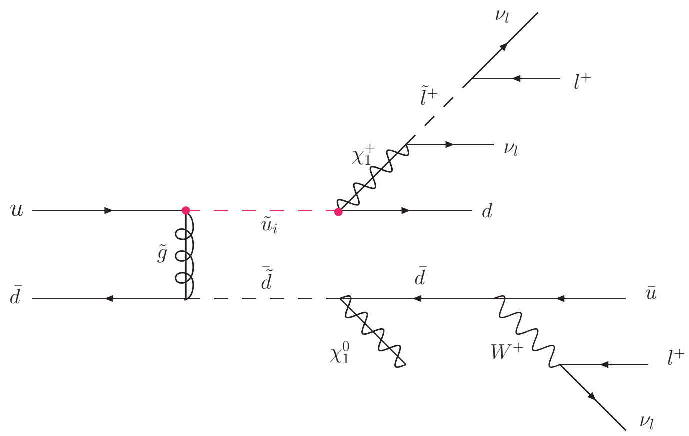

Figure 6.2: An example diagram of type b), in this case $\bar{u} \in \{\bar{u}, \bar{c}\}$ and $d \in \{d, s\}$ are light jets.

where a positively charged lepton can also be produced via an anti-down-type squark. Because the b-tagging efficiencies are multiplied with the cross section, one naively expects that case b) would form less background than a). However, as we will see later these two possibilities can differ quite considerably depending on the phase space region. Although SUSY postulates many new particles, the selection criterion of two same-sign leptons is very restrictive.

Standard Model Backgrounds

Now, we will take processes into account which have already been measured by several experiments. These are present regardless of whether supersymmetry exists or not. Looking at processes within the Standard Model the following two types come into consideration:

a) $VVjj$

b) $t\bar{t}W^+$

The first type a) denotes heavy vector boson pair production accompanied by two quark jets j, with $V \in \{W^+, Z\}$. The W^+ boson should to decay into a lepton and a neutrino, according to [15] with a branching ratio of $BR(W^+ \to l^+\nu_l) = BR(W^+ \to e^+\nu_e) + BR(W^+ \to \mu^+\nu_\mu) = 0.108 + 0.108 = 0.216$ which leaves 4.7% of the total cross section, including decays in both legs. The Z boson can decay into a pair of leptons l^+l^- or neutrinos $\nu_l\bar{\nu}_l$. An event unequal to exactly two l^+ will be discarded, so events are only selected if the l^- can not be detected, e.g. because it escapes in the beam direction. The branching ratio for two charged leptons is [15] $BR(Z \to l^+l^-) = BR(Z \to e^+e^-) + BR(Z \to \mu^+\mu^-) = 3.36\% + 3.37\% = 6.73\%$ per leg, and in total less than 1% of the cross section remains. In our case we have a hierarchy of importance for these backgrounds:

$$W^+W^+jj > W^+Zjj > ZZjj.$$

Because the b quark densities of the proton are very low, the quark jets j are mostly quarks lighter than b quarks and are mis-identified by the detector. Hence, these backgrounds are strongly suppressed. They can be produced either through weak vector boson fusion (VBF) or QCD interactions.

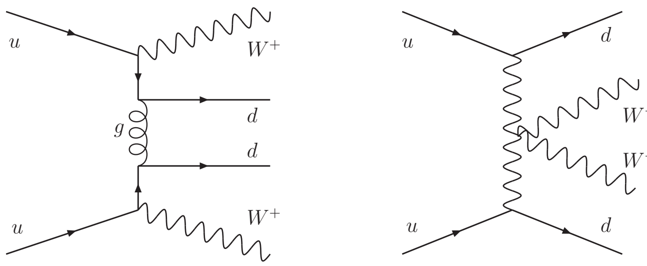

Figure 6.3: Example diagrams of type a) W^+W^+jj, left from QCD, right from VBF.

The Z bosons are produced similar to the W^+ bosons. Due to the strong suppression the $ZZjj$ production can be neglected within the analysis, as we will see in the Chapters 6.3 and 6.4.

A more serious background stems from $t\bar{t}W^+$, whereas the background from $t\bar{t}Z$ production can be neglected because it only counts if the negatively charged lepton gets missed. Due to gluon fusion, pure $t\bar{t}$ production at the LHC7 has a cross section of $143 \pm 14(\text{stat.}) \pm 22(\text{syst.}) \pm 3(\text{lumi.})$ pb [62], which is huge compared to our signal cross section of 6.23 fb. However, $t\bar{t}W^+$ production does not involve initial gluon fusion and therefore, smaller cross sections are obtained, see Figure 6.4. The $t\bar{t}$ pair can be produced in the s-channel via a gluon or through weak interactions. The W^+ boson can be emitted by an initial quark and decay leptonically to one of the two requested positive leptons. The top quarks decay immediately to b quarks and W bosons, because the lifetime is about two orders of magnitude shorter than their hadronisation time. This is due to their large mass of 173.2 GeV [63].

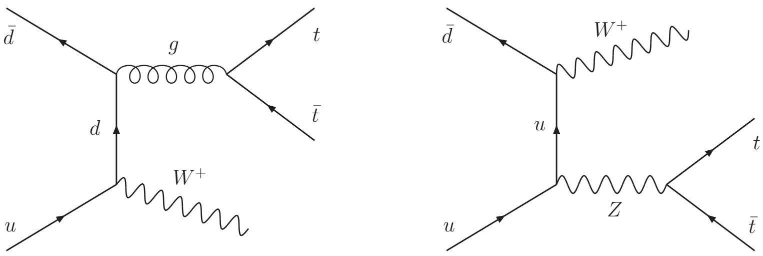

Figure 6.4: Example diagrams for $t\bar{t}W^+$ production.

As presented in Figure 6.4, one final state particle will be a $\bar{b}$ stemming from the $\bar{t}$ and as long as b and $\bar{b}$ are not distinguishable, this process is the main background. The $\bar{b}$ is accompanied by a W^- boson, which can either decay leptonically or hadronically. In the first case it generates a l^- which has to escape the detector in the beam direction. A hadronic decay via a τ^- into pions is possible as well as the direct decay of the W^- into a $q\bar{q}$ pair of light quarks. In the following Chapter we will discuss how this information can be used to reduce the background.

6.2 B-Tagging Efficiencies and Cuts

The LHC is a proton-proton collider and because protons are not elementary particles but consist of partons which initiate the hard process, we have to keep in mind that many remnants of the proton can also take part in reactions. Our analysis is performed at the parton level. Therefore the simulation of hadronisation, parton shower and underlying event has been switched off. This saves a lot of runtime and hardly changes our resulting jets because they are quite central and of high p_T. Nevertheless, we have to implement cuts and b-tagging efficiencies due to the functionality and geometry of the detectors at the LHC.

B-Tagging

B-tagging means the identification of bottom quarks. This can be achieved by detecting the secondary decay vertex of b quarks into lighter particles. Mostly, they form wide jets with high multiplicities. These jets are often, but not always, b jets. Therefore, depending on the phase space region, we assume the following efficiency ϵ per jet in the final state [64]:

ϵ	$30\text{ GeV} < p_{Tb} < 50\text{ GeV}$	$p_{Tb} > 50\text{ GeV}$
$\lvert\eta\rvert < 1.4$	0.65	0.75
$1.4 < \lvert\eta\rvert < 2.4$	0.6	0.7

Table 6.1: B-tagging efficiencies.

A gluon or a light quark jet, meaning u, d, s, or c, can mistakenly be identified as a b jet with a probability of 10%. These values are compatible with recent measurements of ATLAS [65] and CMS [66]. The efficiencies are divided into four phasespace regions depending on the transverse momentum p_T and the pseudorapidity η of the b jet. The pseudorapidity is small for central jets and large for jets in the beam direction. These efficiencies are contained in the rate Γ, which reads:

$$\Gamma = \sigma_{pp\to\tilde{u}_i\tilde{u}_j} \cdot \frac{n}{N} \cdot \epsilon_1 \cdot \epsilon_2 \cdot \int L dt \tag{6.1}$$

where n is the number of selected events, N the number of simulated events, and $\epsilon_{1/2}$ the efficiencies of the two jets. This is used to normalise the histograms so that the contents of all bins add up to the number of events in the detector.

Cuts

The ATLAS as well as the CMS detector is built around the beam and can not register the particles in the beam direction. Therefore, we must exclude these particles by placing cuts on suitable variables. There are common ones usable for almost every process and specific quantities, as e.g. for the $t\bar{t}W^+$ background. The common cuts we have used are:

$$p_{T_{j,l}} > 30\text{ GeV} \qquad |\eta_{j,l}| < 2.4 \qquad \Delta R_{jj}, \Delta R_{ll}, \Delta R_{jl} > 0.4 \tag{6.2}$$

with ΔR measuring the separation of two jets jj and leptons ll, respectively. It is defined as:

$$\Delta R_{ab} := \sqrt{(\eta_a - \eta_b)^2 + (\phi_a - \phi_b)^2}, \tag{6.3}$$

where $\phi_{a,b}$ denotes the azimuthal angle of the particle. The variables $\{a, b\}$ are a generalisation of j and l. Additionally, we can cut on the missing transverse momentum p_T^{miss}. This contains all four-momenta of particles escaping the detector, like neutrinos, neutralinos and particles flying into the beam pipe. The p_T of this sum is quite small when only Standard Model particles contribute. If neutralinos are included, it can become higher than 100 GeV. A common p_T^{miss} cut is set at 100 GeV, but our background can be better suppressed by requiring:

$$p_T^{miss} > 120 \text{ GeV}. \tag{6.4}$$

The most crucial background stems from $t\bar{t}W^+$. However, the decay products of the W^- boson originating from the $\bar{t}$ can be used to reduce this background. The $\bar{t}$ allows for a jet veto of the decaying W^- boson, which can either decay leptonically or hadronically. If it decays into two leptons, the charged ones must have a $p_T < 10$ GeV and $|\eta| > 2.4$, otherwise the event has the wrong signature. These negatively charged leptons and the corresponding neutrinos are added to p_T^{miss}. The alternative is that one of these leptons is a τ, which decays hadronically into pions. It is also possible that the W^- splits up into a pair of quarks, where one must be anti-up- and its partner down-type. These pions and quark jets are vetoed at:

$$p_T^{veto} = 50 \text{ GeV}, \tag{6.5}$$

which means that the event is discarded if the p_T of the additional jets is larger than 50 GeV. This bears a risk, because we are only taking the leading order within perturbation theory into account. In reality, gluons can be radiated, forming additional jets and these events are then mistakenly vetoed as well. These gluon jets would have to be treated within a next-to-leading order (NLO) calculation or a parton shower.

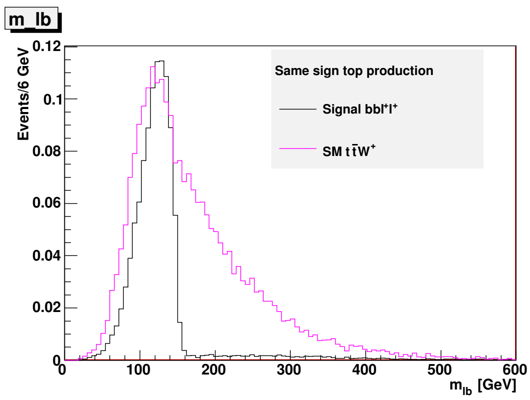

Figure 6.5: Number of events per bin for $\int Ldt = 30$ fb^{-1} at $\sqrt{s} = 7$ TeV plotted versus the invariant mass selection of Equation (6.6), before veto and cut.

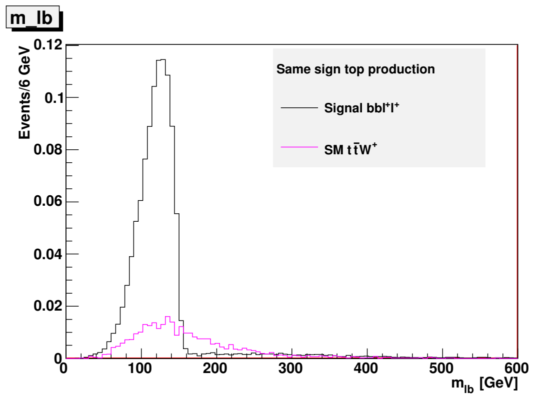

Figure 6.6: Number of events per bin for $\int Ldt = 30$ fb^{-1} at $\sqrt{s} = 7$ TeV plotted versus the invariant mass selection of Equation (6.6), after veto and before cut.

Another important cut concerns the invariant mass m_{bl} of b quark and lepton l^+. If the lepton stems from a top quark, then the invariant mass of the two can at most reach the top quark mass m_t. If the lepton originates from the W^+ which was emitted by an initial state particle, the invariant mass can exceed the value of m_t.

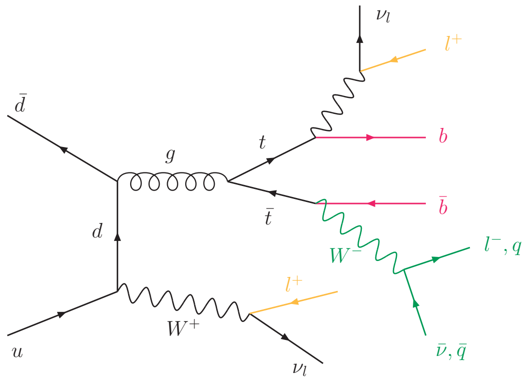

Figure 6.7: $t\bar{t}W^+$ production.

If $m_{bl^+} > m_t$, this event must be a background event and will be discarded, which results from the following selection criterion:

$$\min\{\max\{m_{l_1^+ b_1}, m_{l_2^+ b_2}\}, \max\{m_{l_1^+ b_2}, m_{l_2^+ b_1}\}\} = m_{bl^+} \overset{!}{<} m_t \tag{6.6}$$

The Figures 6.5 and 6.6 show the invariant mass distribution of the bl^+ pair, selected by Equation (6.6). We can see that the jet veto has a very significant effect. The $t\bar{t}W^+$ background can be reduced very well. Figure 6.5 shows, that a lot of background events can be removed by applying a cut to the invariant mass m_{bl^+}. This invariant mass does not include the momentum of the neutrinos and therefore allows for a cut at 150 GeV. However, the veto is more powerful to reduce this background. We will apply both within the following analysis.

Statistics

As we expect only a few events in the detector, we consider them to be Poisson distributed. The distribution equation on the left-hand side of (6.7) approaches a Gaussian distribution in the limit of large numbers. The lower integration bound is minus infinity and the upper one is the desired significance S_P. Therefore, the integrated area covers enough signal events to be S_P standard deviations above the background

$$\sum_{i=0}^{s+b-1} \frac{e^{-b} b^i}{i!} = \int_{-\infty}^{S_P} \frac{e^{-x^2/2}}{\sqrt{2\pi}} dx, \tag{6.7}$$

where b and s denote the number of background and signal events, respectively. This relation is fulfilled by the definition [49]:

$$S_{cL} := \sqrt{2[(s+b)\ln(1+\frac{s}{b}) - s]}, \tag{6.8}$$

which leads to $S_{cl} = s/\sqrt{b}$ for large numbers of b and s. It has been recommended by the CMS design report [50] to use the definition given in Equation (6.8) within an analysis as in the following Chapters.

6.3 Prospects for 7 TeV with $\int Ldt = 30\ \text{fb}^{-1}$

Today, the LHC operates at a center-of-mass energy of 7 TeV and will be upgraded to 14 TeV in 2013/14. In the meantime data will be taken at 8 TeV which can be included to the data set recorded at 7 TeV. We perform the analysis for both cases, 7 TeV and 14 TeV. This makes sense, because we are interested in whether or not the signal of $2b + 2l^+ + E_{miss}^T$ due to NMFV SUSY can already be seen at an intermediate stage. One expects that about $\int Ldt = 30\ \text{fb}^{-1}$ of data will be taken at 7 TeV. We would expect improvements going to higher energies. However, this will be discussed later.

We generated the signal and its supersymmetric background events with Herwig++ [52], whereas the Standard Model background processes have been calculated with Madgraph and Madevent [53]. The analyses, incorporating the selection of events, b-tagging efficiencies and cuts as well as the histograms, have been performed with ROOT [54].

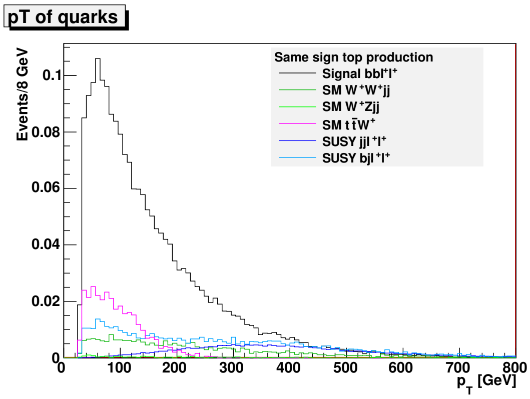

Figure 6.8: Transverse momentum distribution of both b quarks showing the number of events per bin for $\int Ldt = 30\ \text{fb}^{-1}$ at $\sqrt{s} = 7$ TeV. The integrated number of events equals twice the number given in Table 6.2.

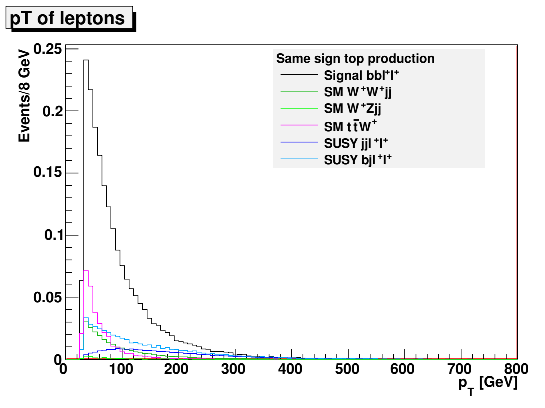

Figure 6.9: Transverse momentum distribution of both leptons l^+ showing the number of events per bin for $\int Ldt = 30\ \text{fb}^{-1}$ at $\sqrt{s} = 7$ TeV. The integrated number of events equals twice the number given in Table 6.2.

On the vertical axis the simulated event numbers in the detector are shown, depending on the transverse momentum p_T of the b quarks and leptons, respectively. The black line corresponds to the signal process and refers to a total event number of 0.99. Unfortunately, this is only just about one event and taking Poisson statistics into account, might not be produced at all. Nevertheless, the signal dominates the several backgrounds and we obtain the following detector events and the significance S_{cL}:

Signal	SM BG			SUSY BG		Significance
bbl^+l^+	$t\bar{t}W^+$	W^+W^+jj	W^+Zjj	bjl^+l^+	jjl^+l^+	S_{cL}
0.99	0.16	0.12	0.007	0.27	0.11	1.05σ

Table 6.2: Simulated number of events registered by the detector.

The most important background stems from $t\bar{t}W^+$. Here we have taken b and $\bar{b}$ into account, by making the assumption of being unable to distinguish between them. It is the only process containing a b anti-quark. The other backgrounds due to SM interactions correspond to the green lines and are very low. The blue curves show the background from SUSY, where either one light quark jet or both have been mis-tagged. There is a peak in the light blue curve at low p_T, which refers to the one real b quark. Light quark jets mostly stem from heavy squark mass eigenstates $\tilde{u}_2, ..., \tilde{u}_5$ and result in light quarks with large p_T. Most b quarks are produced via the $\tilde{u}_1$, some via $\tilde{u}_6$, remembering that in the flavour conserving case $\tilde{u}_1 = \tilde{u}_L$ and $\tilde{u}_6 = \tilde{t}_R$. The "13" mixing allows for the transition to top quarks, by emitting a neutralino χ_1^0. Comparing the b and lepton jets, the curves have similar behaviour, but the leptons carry roughly half the p_T of the b jets. The next plots, Figure 6.10 and 6.11, present the p_T spectrum of the two b jets separately, the one with lower p_T is shown on the left, the high-p_T b jet is shown on the right.

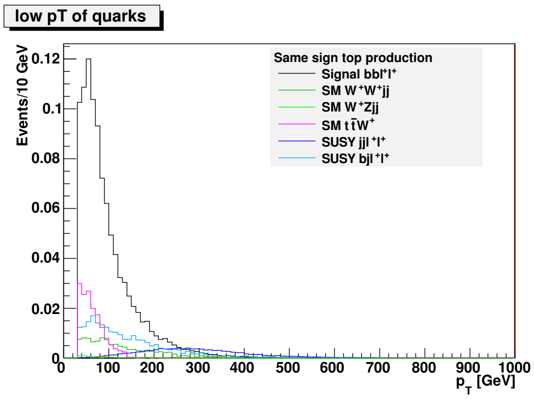

Figure 6.10: Transverse momentum distribution of the b jet with lower p_T showing the number of events per bin for $\int Ldt = 30$ fb^{-1} at $\sqrt{s} = 7$ TeV.

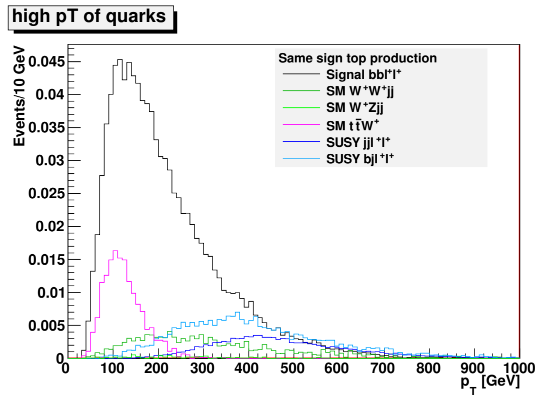

Figure 6.11: Transverse momentum distribution of the b jet with higher p_T showing the number of events per bin for $\int Ldt = 30$ fb^{-1} at $\sqrt{s} = 7$ TeV.

The signal remains as the dominant curve here, too. The shape of the light blue SUSY bjl^+l^+ curves indicate a soft p_T distribution, whereas the dark blue curves of the SUSY jjl^+l^+ background show a hard p_T distribution. However, we can see from the signal curve that the b jets can also have quite a large p_T.

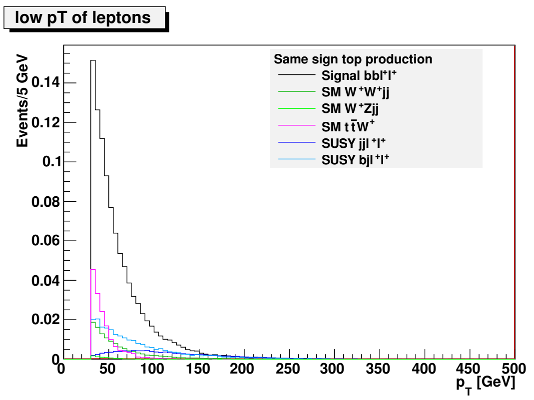

Figure 6.12: Transverse momentum distribution of the lepton with lower p_T showing the number of events per bin for $\int Ldt = 30$ fb^{-1} at $\sqrt{s} = 7$ TeV.

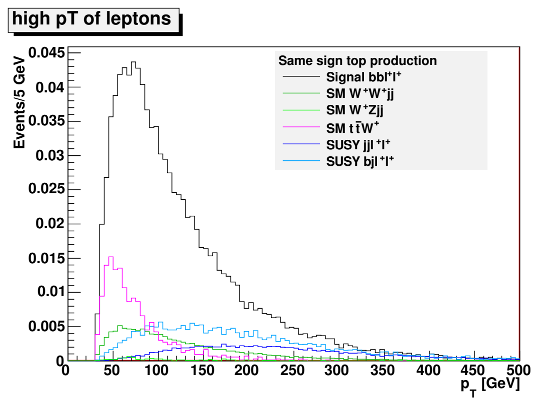

Figure 6.13: Transverse momentum distribution of the lepton with higher p_T showing the number of events per bin for $\int Ldt = 30$ fb^{-1} at $\sqrt{s} = 7$ TeV.

The same discussion can be applied to the leptons, see Figure 6.12 and 6.13. As the shapes of the signal and the background curves have a similar shape, it will be difficult to distinguish them in the experiment. We look next at the distribution of the pseudorapidity, Figures 6.14, 6.15. The b jets as well as the leptons are emitted centrally and therefore, suitable to be registered by the detectors. Although taking processes via vector boson fusion into account, the contributions from QCD wash out the so-called rapidity gap.

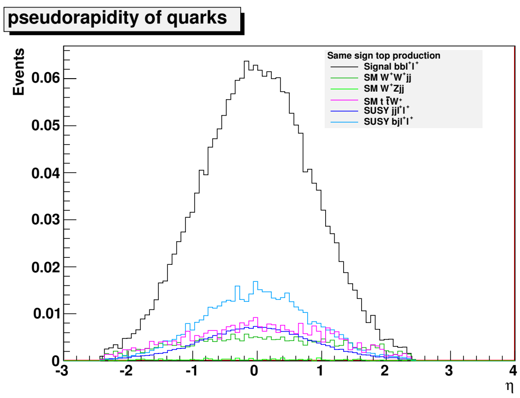

Figure 6.14: Pseudorapidity distribution of the two b jets showing the number of events per bin for $\int Ldt = 30$ fb^{-1} at $\sqrt{s} = 7$ TeV. The integrated number of events equals twice the number given in Table 6.2.

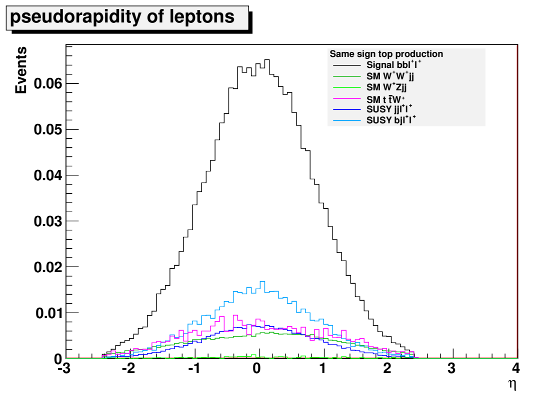

Figure 6.15: Pseudorapidity distribution of the two leptons showing the number of events per bin for $\int Ldt = 30$ fb^{-1} at $\sqrt{s} = 7$ TeV. The integrated number of events equals twice the number given in Table 6.2.

So far we did not consider the information from the undetectable final state particles, e.g. neutralinos χ_1^0, neutrinos ν_l and particles which escape the detector in the direction of the beam pipe. Energy momentum conservation holds at each vertex and therefore, we can reconstruct them through the missing momentum of each event. In general, the sum of their momenta corresponds to the negative sum of the momenta of all visible particles. By measuring the vectorial sum of the p_T of all visible particles we also get the combined p_T of all invisible particles, that is to say the p_T^{miss}. Having performed Monte Carlo based simulations, we can alternatively add up all four momenta of missed particles, these are written down in the event files and study the transverse momentum of this summed vector, see Figure 6.16. We can see the cut at 120 GeV to dispose of some of the background, mainly from $t\bar{t}W^+$ and W^+W^+jj and that the signal dominates the background.

Figure 6.17 presents the b quarks' p_T distribution of the signal (black) versus the total background (red). The background dominates above a p_T of 350 GeV and is due to the SUSY background jjl^+l^+. In the low p_T region, background and signal behave similarly which is unusual for processes within supersymmetry. By applying the cuts of Chapter 6.2, the SM background can be suppressed very well. To summarise, the best region to explore same-sign top production through NMFV within squark pair production via a gluino exchange in the t-channel, is below 300 GeV in the p_T distribution or by studying the missing transverse momentum distribution.

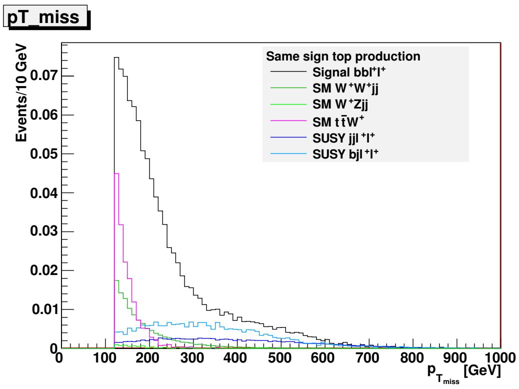

Figure 6.16: Missing transverse momentum distribution of the signal compared to its backgrounds showing the number of events per bin for $\int Ldt = 30$ fb^{-1} at $\sqrt{s} = 7$ TeV.

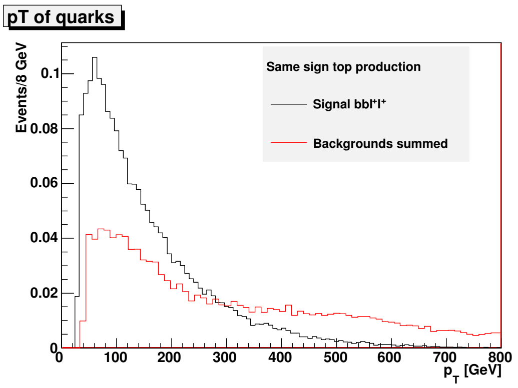

Figure 6.17: Transverse momentum distribution of both b quarks of the signal compared to the summed backgrounds showing the number of events per bin for $\int Ldt = 30$ fb^{-1} at $\sqrt{s} = 7$ TeV. The integrated number of events equals twice the number given in Table 6.2.

6.4 Prospects for 14 TeV with $\int Ldt = 100$ fb^{-1}

The last Chapter was addressed to the exploration of the signal process at the LHC7. Now we will raise the energy and the integrated luminosity. As mentioned at the beginning of Chapter 6.3, we expect improvements in the number of events and the significance. To reduce the $t\bar{t}W^+$ background, we cut the missing transverse momentum at:

$$p_T^{miss} > 140 \text{ GeV}. \tag{6.9}$$

All other cuts and b-tagging efficiencies are the same as in Chapter 6.3. The Figures 6.18 and 6.19 show the p_T distributions of the b quarks and leptons l^+.

Relative to the black curve of the signal, the green coloured SM backgrounds, namely W^+W^+jj and W^+Zjj shrink. The background stemming from $t\bar{t}W^+$ has risen similar to the signal, but the SUSY background increased strongly. This is due to the fact that the parton densities, as described earlier in Figure 5.7, behave differently at high energies. Now, the gluon fusion subprocess $gg \to \tilde{u}_1\bar{\tilde{u}}_1$ has more impact, whereas $uu \to \tilde{u}_1\tilde{u}_1, \tilde{u}_1\tilde{u}_6$ have decreased. All in all, relative to the number of b quarks, more light quarks are produced that can be mis-identified. Table 6.3 shows the number of events in the detector and the significance.

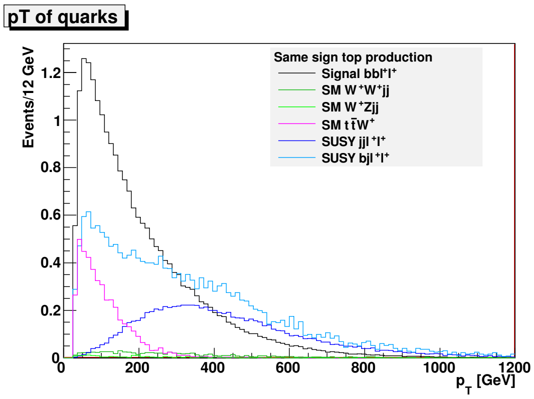

Figure 6.18: Transverse momentum distribution of both b quarks showing the number of events per bin for $\int Ldt = 100$ fb^{-1} at $\sqrt{s} = 14$ TeV. The integrated number of events equals twice the number given in Table 6.3.

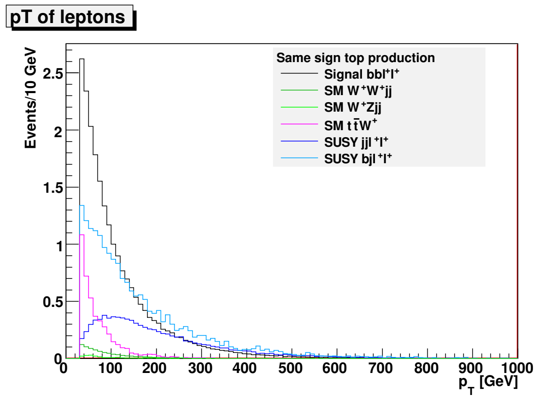

Figure 6.19: Transverse momentum distribution of both leptons l^+ showing the number of events per bin for $\int Ldt = 100$ fb^{-1} at $\sqrt{s} = 14$ TeV. The integrated number of events equals twice the number given in Table 6.3.

Signal	SM BG			SUSY BG		Significance
bbl^+l^+	$t\bar{t}W^+$	W^+W^+jj	W^+Zjj	bjl^+l^+	jjl^+l^+	S_{cL}
11.04	2.17	0.43	0.10	9.67	4.43	2.46σ

Table 6.3: Simulated number of events registered by the detector.

Compared to the event numbers in Table 6.2 at $\sqrt{s} = 7$ TeV and $\int Ldt = 30$ fb^{-1}, several events are produced. Despite the fact that the background dominates most regions, as shown in Figure 6.24, we still obtain a significance S_{cL} of 2.46σ. The p_T distributions of the discrete bottom quark jets and leptons are presented in Figures 6.20, 6.21, 6.22 and 6.23. Their behaviour is similar to what was found at $\sqrt{s} = 7$ TeV.

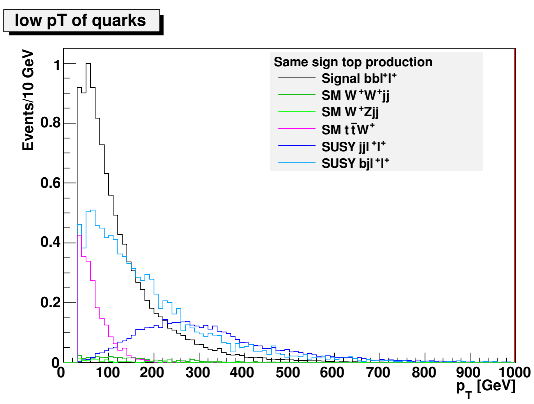

Figure 6.20: Transverse momentum distribution of the b jet with lower p_T showing the number of events per bin for $\int Ldt = 100$ fb^{-1} at $\sqrt{s} = 14$ TeV.

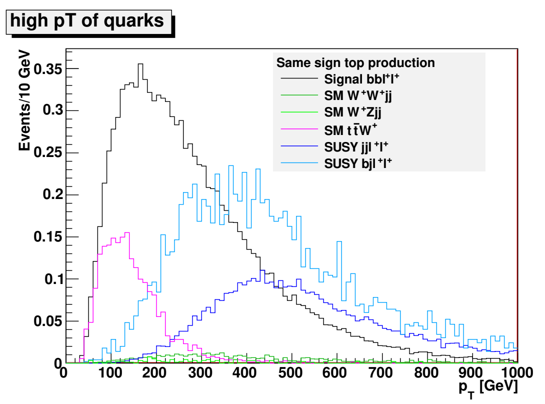

Figure 6.21: Transverse momentum distribution of the b jet with higher p_T showing the number of events per bin for $\int Ldt = 100$ fb^{-1} at $\sqrt{s} = 14$ TeV.

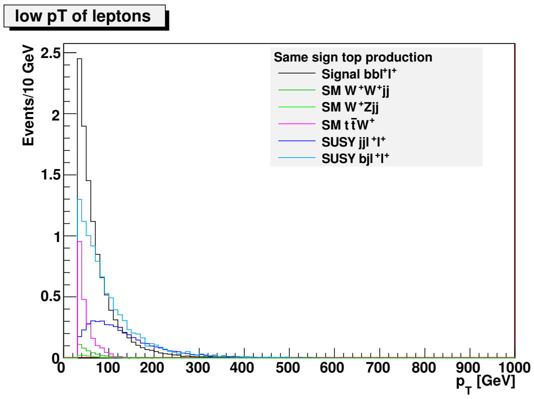

Figure 6.22: Transverse momentum distribution of the lepton with lower p_T showing the number of events per bin for $\int Ldt = 100$ fb^{-1} at $\sqrt{s} = 14$ TeV.

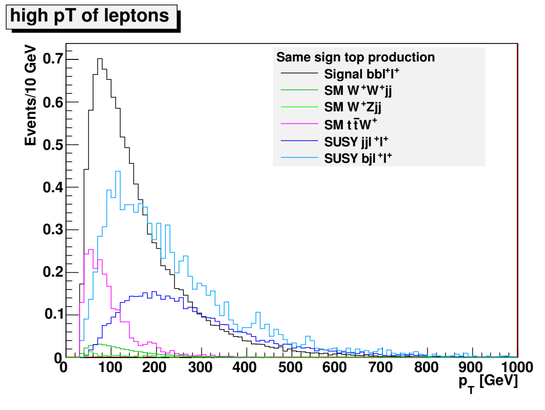

Figure 6.23: Transverse momentum distribution of the lepton with higher p_T showing the number of events per bin for $\int Ldt = 100$ fb^{-1} at $\sqrt{s} = 14$ TeV.

Looking at the p_T^{miss} distributions is a popular way of searching for heavy new particles, because the backgrounds from the SM mostly contain neutrinos and their production falls off rapidly with rising energy. Whereas if very heavy particles are involved the cross section rises at high energies. As our background from SUSY is quite dominant, we can not use this distribution as we had hoped to at the beginning, see Figure 6.25.

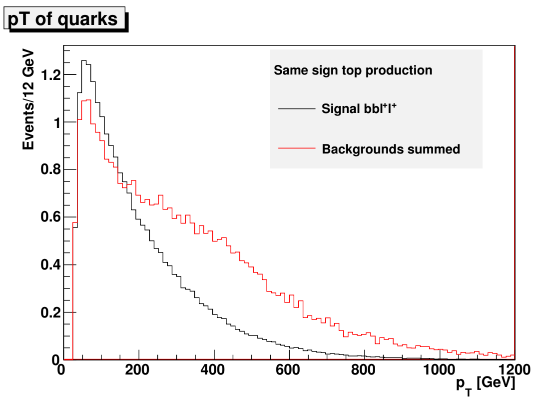

Figure 6.24: Transverse momentum distribution of both b quarks of the signal compared to the summed backgrounds showing the number of events per bin for $\int Ldt = 100$ fb^{-1} at $\sqrt{s} = 14$ TeV. The integrated number of events equals twice the number given in Table 6.3.

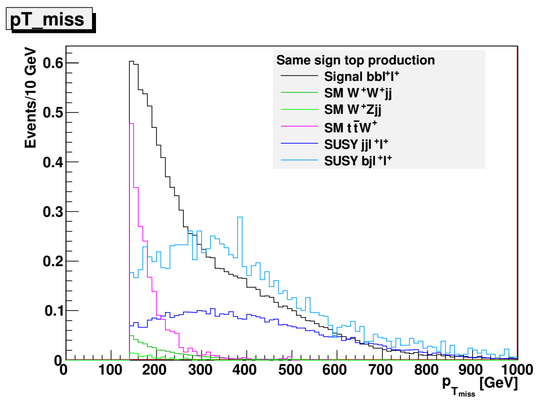

Figure 6.25: Missing transverse momentum distribution of the signal compared to the backgrounds showing the number of events per bin for $\int Ldt = 100$ fb^{-1} at $\sqrt{s} = 14$ TeV.

6.5 Comparison to Recent Experimental Studies at 7 TeV

As previously stated, supersymmetry has not yet been discovered at the LHC. However, many searches are ongoing, for example in the channel of two same-sign leptons accompanied by two or more jets. We have discussed the case of more than two b-tagged jets in Chapter 4. Now we will discuss the flavour conserving (FC) generation of exactly two jets within the final state and compare it to the flavour violating (FV) production. The corresponding mass spectra are given in Table 6.4 and 6.5. Note, that the average of the squark masses of both scenarios differ by merely 30 GeV, which allows for a comparison of both scenarios.

FV	χ_1^0	χ_2^0	χ_1^+	$\tilde{g}$	$\tilde{u}_1$	$\tilde{u}_2$	$\tilde{u}_3$	$\tilde{u}_4$	$\tilde{u}_5$	$\tilde{u}_6$	$\bar{m}_{\tilde{u}}$
m/GeV	138	494	494	2000	398	787	993	1013	1051	1184	904

Table 6.4: Neutralino, chargino, gluino and squark masses produced by input values in Table 5.5 and Equation (5.6) via FV. The last column shows the averaged squark mass. This spectrum is the same as in Chapter 5.5.

FC	χ_1^0	χ_2^0	χ_1^+	$\tilde{g}$	$\tilde{u}_1$	$\tilde{u}_2$	$\tilde{u}_3$	$\tilde{u}_4$	$\tilde{u}_5$	$\tilde{u}_6$	$\bar{m}_{\tilde{u}}$
m/GeV	138	494	494	2000	787	792	964	994	1014	1052	934

Table 6.5: Neutralino, chargino, gluino and squark masses produced by input values in Table 5.5 and flavour conserving (FC). The last column shows the averaged squark mass.

In the conclusion of [3], it was supposed that "... in the squark search one should take into account the possibility of significant contributions from QFV squark decays". We will check this with our signal process $pp \to 2t + 2\chi_1^0 \to 2j + 2l^+ + E_T^{miss}$.

Without b-Tagging

In Chapter 6.3 we saw that b-tagging can improve the significance of the signal tremendously. To gain as many events as possible we will switch off the b-tagging and take all quark jets into account. This means that the background from SUSY, which was due to mis-tagging in Chapter 6.1, is now added to the signal process as well. We compare the curve of the flavour conserving production of the signal (black) to the flavour violating one (blue), see Figures 6.26 and 6.27.

We did not implement the jet veto of Equation (6.5). This is due to the fact that we do not focus on the tagging of b jets. The additional jets can not be identified as confidently and moreover, the background from $t\bar{t}W^+$ is not as immense as in the two Chapters before. Besides this it is suppressed fairly well by the invariant mass cut, see Equation (6.6). The dominant background stems from the W^+W^+jj channel and not from $t\bar{t}W^+$. To reduce it we made a stronger cut on the missing transverse momentum:

$$p_T^{miss} > 160 \text{ GeV}. \tag{6.10}$$

In Figure 6.26 the SM jets are rather soft, which is typical for SM processes, whereas the maxima of the supersymmetric production are located at higher transverse momenta. The FV curve lies above the FC one, which means that more events have been produced. This is due to the mixing and therefore a larger mass splitting of the squark mass eigenstates. The

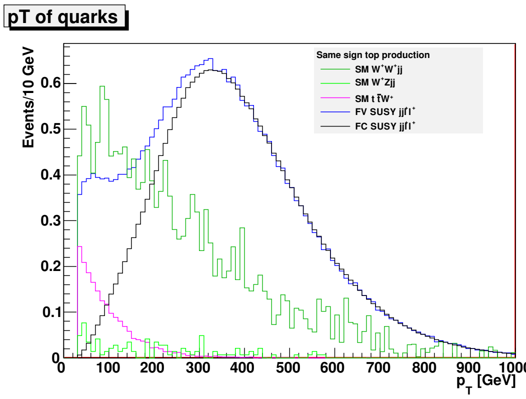

Figure 6.26: Transverse momentum distribution of both b quarks showing the number of events per bin for $\int Ldt = 30 \text{ fb}^{-1}$ at $\sqrt{s} = 7$ TeV. The integrated number of events equals twice the number given in Table 6.6.

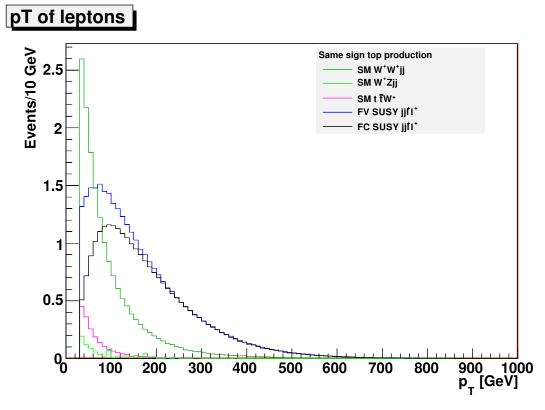

Figure 6.27: Transverse momentum distribution of both leptons l^+ showing the number of events per bin for $\int Ldt = 30 \text{ fb}^{-1}$ at $\sqrt{s} = 7$ TeV. The integrated number of events equals twice the number given in Table 6.6.

$\tilde{u}_1$ within FV is only 398 GeV, while $m_{\tilde{u}_1} = 787$ GeV by assuming FC. The first case is more likely to be produced and leads, via the mixing, to b quarks in the final state. These show up as a low peak in the blue curve at 100 GeV, which is consistent with the low peak (blue) in Figure 6.28 and no peak in Figure 6.29 around 100 GeV.

Signal FV	Signal FC	SM BG			Significance	
jjl^+l^+	jjl^+l^+	W^+W^+jj	$t\bar{t}W^+$	W^+Zjj	S_{cL} FV	S_{cL} FC
14.71	12.43	8.35	0.95	0.40	3.95σ	3.41σ

Table 6.6: Simulated number of events registered by the detector.

NMFV changes the shape of the distribution marginally. Unfortunately, the low p_T region of the signal is coverd by a large amount of background coming from W^+W^+jj, making it difficult to extract the signal. Nevertheless, we get a significance of more than 3σ in both cases.

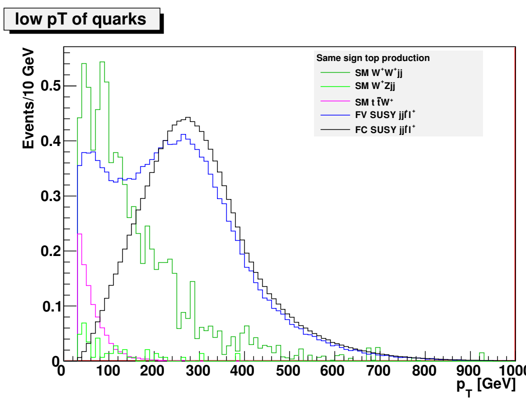

Figure 6.28: Transverse momentum distribution of the b jet with lower p_T showing the number of events per bin for $\int Ldt = 30 \text{ fb}^{-1}$ at $\sqrt{s} = 7$ TeV.

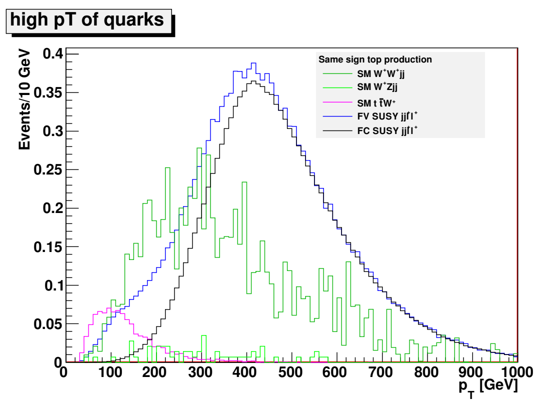

Figure 6.29: Transverse momentum distribution of the b jet with higher p_T showing the number of events per bin for $\int Ldt = 30 \text{ fb}^{-1}$ at $\sqrt{s} = 7$ TeV.

Even the missing p_T distribution in Figure 6.30 shows that the two scenarios are hardly distinguishable from one another. It seems that NMFV would not influence the discovery within this channel. To find out, whether SUSY would incorporate flavour violation beyond the CKM mixing, further investigations are necessary. For example an analysis as we presented in Chapter 6.3 and 6.4.

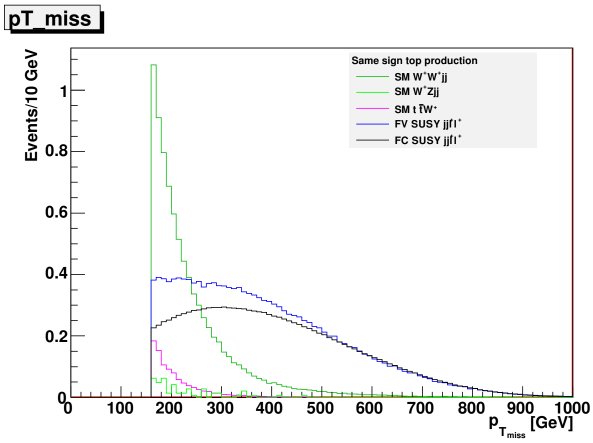

Figure 6.30: Missing transverse momentum distribution of the signal compared to its backgrounds showing the number of events per bin for $\int Ldt = 30\ \mathrm{fb}^{-1}$ at $\sqrt{s} = 7$ TeV.

6.6 Discussion

In Chapter 6.4 we could produce a signal with a significance of $S_{cL} = 2.46\sigma$. Unfortunately, this is not enough for a discovery, which requires at least 5σ evidence. We found out that the flavour non-violating SUSY background is more problematic than the SM background. However, the ratio of signal to background is better at $\sqrt{s} = 7$ TeV. Therefore, it would be interesting to collect more than $\int Ldt = 30\ \mathrm{fb}^{-1}$ of data. This is not planned to be carried out at 7 TeV within the next few years. Nevertheless, it might be worth studying further in the future when evidence for supersymmetry is available. Then one might even be able to distinguish between b and $\bar{b}$ quarks and drastically reduce the background from $t\bar{t}W^+$. We have shown in Chapter 6.5 that even though NMFV does not have an impact on the discovery process of supersymmetry $pp \to 2j + 2l^+ + E_T^{miss}$, it makes sense to perform an analysis of same-sign top production to explore the flavour violating characteristic of supersymmetry.

CHAPTER 7

Conclusion

This work is aimed at the phenomenology of the non-minimal flavour violating minimal supersymmetric model. So far, no evidence exists as to whether further flavour violation, beyond the well-known CKM mixing, is realized in nature or not. From a theoretical point of view it arises naturally from breaking supersymmetry softly and can be suppressed by assumptions regarding the breaking mechanism. These are often simplifications which reduce the 6×6 dimensional mixing matrix to a 2×2 dimensional matrix. To date, the experiments ATLAS and CMS have been able to exclude a large range of parameters within such simplified models [44, 45]. This raises the interest of more general and therefore more complicated models, e.g. including non-minimal flavour violation. The naturalness argument that physics ought to be a synergy of simpleness, elegance and precision might not be achieved by todays ideas. Nevertheless, every theory should be studied and well-understood to be able to match it to nature. This affords the prediction of observables and adequate experiments, as e.g. the LHC which gives us an access to nature.

We have studied the signal process $2b + 2l^+ + E_T^{miss}$. For this purpose we explored mixing between the first and third generation of squarks, being the scalar supersymmetric partners of quarks. This mixing allows for transitions of quarks to squarks via exchanging a gluino in the t-channel. By choosing maximal parameters δ_{13}^{LR} and δ_{13}^{RR} we can produce squark mass eigenstates consisting of a fairly large part of top squark flavour. This enhances the probability of the squark to decay into a top quark and a neutralino. Incidentally, this neutralino is the lightest supersymmetric and therefore, a stable particle which serves as a candidate for a dark matter particle. It is a well-known fact, that top quarks decay exclusively to bottom quarks and W bosons, due to their large mass. The second heaviest, but very much lighter quarks, are bottom quarks. These can be identified quite easily by a detector and are suitable as observable final state particles. As we are producing same-sign top quarks, we have every particle twice, especially two same-sign leptons, coming from the decay of the W^+ bosons. Invisible particles were collected to the observable p_T^{miss}.

In Chapters 2 and 3 we briefly introduced the underlying theory of this work, namely the Standard Model and its supersymmetrisation, the minimal supersymmetric standard model and the sources of flavour violation. It was very important to check whether the choice of flavour violating parameters does not contradict any measurements. These constraints have been studied in Chapter 4. In contrast to transitions between the second and third, the ones between the first and third particle generation are very unlikely in the Standard Model. Hence, measurements of flavour changing neutral current processes have quite large uncertainties. This means that a larger range of parameters concerning flavour violation in the MSSM is still allowed. Besides low energy observables from B-Physics we checked against recent exclusion limits from the LHC and so-called vacuum stability conditions. The latter are required from theory to support charge and colour conservation. These constraints yielded us a benchmark point, which is consistent with our recent experimental knowledge of particle physics. Since they are quite loose, we could achieve a sizable mixing.

After we have excluded certain regions of parameters, we were left with the remaining ones. Because we have not yet seen any evidence of supersymmetry, we decided to explore the best situation. In Chapter 5 we searched the set of parameters which leads to the biggest total cross section of the signal process. As neither the theory nor experiments prefer an ascending or descending mass hierarchy of squarks, we took the one which leads to the most promising perspective considering the case that further parameters might be excluded in the not too distant future. Our study concluded that the most significant analysis can be achieved by the set of parameters:

$$(\delta_{13}^{RR}|\delta_{13}^{LR}) = (0.803|0.055).$$

Recently, a number of analyses concerning relatively light third generation squarks appeared. Therefore, we also studied an effective supersymmetric scenario. However, the result turned out to be negligible.

The main issue was to perform a LHC Monte Carlo analysis of the process $pp \to 2t + 2\chi_1^0 \to 2b + 2l^+ + E_{miss}^T$, taking mixing between the first and third particle generation into account. In [3] mixing between the second and third generation enhanced the channel $pp \to c\bar{t}(t\bar{c}) + E_{miss}^T + X$ and the suggestion was to include such an effect in recent searches for squarks. We did this for the signal process mentioned above and at least in our case, could not agree with their speculation. In Chapter 6.5 we saw an excess below a transverse momentum of 150 GeV of bottom quarks due to our mixing parameters. These are not present when assuming flavour conserving squark pair production via a gluino exchange in the t-channel. However, the peak lies below the peak of background stemming from jjW^+W^+ and is therefore hard to discover.

In Chapter 6.3 we studied the signal $pp \to 2b + 2l^+ + E_T^{miss}$ at a center-of-mass energy of $\sqrt{s} = 7$ TeV and an integrated luminosity of $\int Ldt = 30$ fb^{-1}. By tagging the bottom quark jets and requiring exactly two same-sign leptons we tried to gain a very significant signal. Except for top quark production, the direct production of bottom quarks in our case is very unlikely because their parton densities are very low. Light quarks are produced preferably and sometimes mis-identified as bottom quarks by the detector. This can happen to events produced by Standard Model interactions as well as to ones generated via intermediate supersymmetric particles. The main background was due to the $t\bar{t}W^+$ process. We did not distinguish between bottom quarks and their anti-particles. As this is an obvious difference to the actual signal, it might be a reducible background in the future, when one is able to distinguish b and $\bar{b}$ in the detector. This would make our signal much more significant. So far, we have achieved a significance of $S_{cL} = 1.05\sigma$.

After exploring the signal at the intermediate energy of $\sqrt{s} = 7$ TeV, we went on to 14 TeV and $\int Ldt = 100$ fb^{-1} in order to improve the significance. The choice of the benchmark point then lead to 11 signal events and a significance of $S_{cL} = 2.46\sigma$. Indeed, this is an improvement, but not as good as we had previously expected. Relative to the signal, we produced more supersymmetric background events. The signal went up with an overall factor of 11 and the supersymmetric backgrounds with 37, whereas the Standard Model backgrounds have only risen by a factor of roughly 9. Compared to the situation at $\sqrt{s} = 7$ TeV, raising the beam energy has a less positive effect than collecting more data.

Finally, we studied whether or not non-minimal flavour violation has an effect on current searches for squarks, as suggested in [3]. For this purpose we abandoned b-tagging and studied the signal $pp \to 2j + 2l^+ + E^T_{miss}$, produced via flavour violating and via flavour conserving squark pair production, respectively. The difference appeared as a peak around 60 GeV in the transverse momentum distribution of the flavour violating process. Moreover, non-minimal flavour violation led to an enhanced distribution of the missing transverse momentum. Overall, the flavour violating process with 3.95σ is slightly more significant than the flavour conserving one with 3.41σ. However, this is not a remarkable improvement. To find out whether or not non-minimal flavour violation is realized within supersymmetry, it is appropriate to perform a specialised analysis, e.g. as presented in Chapter 6.3.

In summary, non-minimal flavour violation would hardly influence current searches for squarks via the signal of $2j + 2l^+ + E_T^{miss}$. However, if supersymmetry will have been discovered, an analysis of same-sign top production leading to $2b+2l^+ +E_T^{miss}$ in the final state seems viable. Especially, as soon as one is able to distinguish bottom quarks and their anti-particles, this process is appropriate to determine flavour violating parameters and might be useful to pin down the breaking mechanism of supersymmetry.

References

[1] J.W. von Goethe. *Faust, A Tragedy.* Translated by G.M. Priest. http://www.levity.com/alchemy/faust02.html 2/03/2012

[2] M. Spannowsky. *LHC Higgs Physics beyond the Standard Model.* Dissertation, LMU München, (2007).

[3] Porod et al.. *Impact of squark generation mixing on the search for squarks decaying into fermions at LHC.* Phys.Lett.B698:380-388, (2011).

[4] G. Zweig. *An SU3 model for strong interaction symmetry and its breaking.* Developments in the Quark Theory of Hadrons, pp.22-101, 1964.

[5] S.L. Glashow, M. Gell-Mann. *Gauge Theories Of Vector Particles.* Annals Phys. 15 (1961) 437-460.

[6] S. Weinberg. *A Model of Leptons.* Phys.Rev.Lett. 19 (1967) 1264-1266

[7] A. Salam, J.C. Pati. *Unified Lepton-Hadron Symmetry and a Gauge Theory of the Basic Interactions.* Phys.Rev. D8 (1973) 1240-1251.

[8] Franz Mandl, Graham Shaw. *Quantum Field Theory.* Wiley, 2nd Edition, 2010.

[9] Paul Langacker. *Structure of the Standard Model.* arXiv:hep-ph/0304186v1.

[10] Graphic from Desy. http://www.weltmaschine.de/e92/e70729/e75761/ 06/03/2012

[11] P.W. Higgs. *Spontaneous Symmetry Breakdown without Massless Bosons.* Phys. Rev. 145, 1156–1163 (1966)

[12] F. Englert, R. Brout. *Broken Symmetry and the Mass of Gauge Vector Mesons.* Phys.Rev.Lett. 13 (1964) 321-323

[13] T.W.B. Kibble. *Symmetry Breaking in Non-Abelian Gauge Theories.* Phys. Rev. 155, 1554–1561 (1967)

[14] J.C. Collins, D.E. Soper, G. Sterman. *Factorization of Hard Processes in QCD.* Adv.Ser.Direct.High Energy Phys.5:1-91, (1988).

[15] Particle Data Group. http://pdg.lbl.gov/ 07/03/2012

[16] Graphic by D.I. Kazakov. (2001). http://leyton.web.cern.ch/leyton/why.html 17/11/2011

[17] F. Zwicky. *On the Masses of Nebulae and of Clusters of Nebulae.* Astrophys.J. 86 (1937) 217-246.

[18] Graphic by Nasa. http://map.gsfc.nasa.gov/media/080998/index.html 17/11/2011

[19] P.J.E. Peebles, Bharat Ratra. *The Cosmological Constant and Dark Energy.* Rev.Mod.Phys.75:559-606 (2003).

[20] A.G. Riess, et al.. *Observational Evidence from Supernovae for an Accelerating Universe and a Cosmological Constant.* Astron. J. 116 1009 (1999).

[21] Graphic by Nasa. http://wmap.gsfc.nasa.gov/media/101080/ 17/11/2011

[22] L. Bergström. *Non-baryonic dark matter: observational evidence and detection methods.* Rep. Prog. Phys. 63 793 (2000).

[23] H. Kalka, G. Soff. *Supersymmetrie.* Teubner Verlag.

[24] M. Mühlleitner. *Supersymmetry an Collidern.* http://www-itp.particle.uni-karlsruhe.de/ maggie/susycolliders11/

[25] Updated October 2011 by K. Nakamura, S.T. Petcov. *Neutrino mass, mixing, and flavor change* Chapter 13, PDG 2011.

[26] S. Coleman, J. Mandula. *All Possible Symmetries of the S Matrix.* Phys. Rev. 159, 1251–1256 (1967).

[27] R. Haag, J.T. Lopuszanski, M. Sohnius. *All possible generators of supersymmetries of the S-matrix.* Nucl. Phys., B88:257 (1975).

[28] J. Lopuszanski. *An Introduction to Symmetry and Supersymmetry in Quantum Field Theory.* World Scientific, 1991.

[29] T. Fritzsche. *Untersuchungen zum Massenspektrum von Neutralinos und Charginos im Minimalen Supersymmetrischen Standardmodell.* Diploma thesis. http://www-itp.particle.uni-karlsruhe.de/diplomatheses.de.shtml 07/03/2012

[30] L. Girardello, M.T. Grisaru. *Soft breaking of supersymmetry.* Nucl. Phys., B194:1 (1982).

[31] M. Drees, R. Godbole, P. Roy. *Theory and Phenomenology of Sparicles.* Page 197ff, World Scientific Pub Co Inc (2004).

[32] W. Porod. *SPheno, a program for calculating supersymmetric spectra, SUSY particle decays and SUSY particle production at e+ e- colliders.* Comput.Phys.Commun.153:275-315, (2003).

[33] E. Fermi. *An attempt of a theory of beta radiation. 1..* Z.Phys. 88 (1934) 161-177

[34] M. Arana-Catania, S. Heinemeyer, M.J. Herrero, S. Penaranda. *Higgs Boson masses and B-Physics Constraints in Non-Minimal Flavor Violating SUSY scenarios.* arXiv:1109.6232v2 [hep-ph]

[35] C. Bobeth, T. Ewerth, F. Krüger, J. Urban *Enhancement of* $Br(B_d \to mu^+mu^-)/Br(B_s \to mu^+mu^-)$ *in the MSSM with Modified Minimal Flavour Violation and Large tan(beta).* Phys.Rev.D66:074021, (2002).

[36] T. Hahn. *Generating Feynman Diagrams and Amplitues with FeynArts 3.* Comput.Phys.Commun. 140 418-431 (2001).

[37] T. Huber, E. Lunghi, M. Misiak, D. Wyler. *Electromagnetic Logarithms in* $B \to X_s l + l-$. Nucl.Phys.B740:105-137, (2006).

[38] Heavy Flavor Averaging Group. http://www.slac.stanford.edu/xorg/hfag/ 07/03/2012

[39] D.A. Ross, M. Veltman. *Neutral Currents and the Higgs Mechanism.* Nucl. Phys. B95 (1975) 135-147.

[40] M. Böhm, A. Denner, H. Joos. *Gauge theories of the strong and electroweak interaction.*

[41] J.A. Casas, S. Dimopoulos. *Stability Bounds on Flavor-Violating Trilinear Soft Terms in the MSSM.* Phys.Lett. B387 107-112 (1996).

[42] CDF and D0 Collaboration. *Seeking the Brout-Englert-Higgs Boson.* Talk given at Rencontres de Moriond, March 2012, Italy, by W. Fisher.

[43] CMS Collaboration. *Combined results of searches for the standard model Higgs boson in pp collisions at* $\sqrt{s} = 7\ TeV$. arXiv:1202.1488v1 [hep-ex]

[44] ATLAS Collaboration. https://twiki.cern.ch/twiki/bin/view/AtlasPublic/CombinedSummaryPlots 16/12/2011

[45] CMS Collaboration. https://twiki.cern.ch/twiki/bin/view/CMSPublic/PhysicsResultsSUS 16/12/2011.

[46] CMS Collaboration. https://twiki.cern.ch/twiki/bin/view/CMSPublic/PhysicsResultsSUS11020 28/03/2012

[47] P. Skands et al.. *SUSY Les Houches Accord: Interfacing SUSY Spectrum Calculators, Decay Packages, and Event Generators.* JHEP 0407:036,2004.

[48] B.C. Allanach et al.. *SUSY Les Houches Accord 2.* Comp.Phys.Commun.180:8-25,2009.

[49] J.R. Espinosa, C. Grojean, M. Mühlleitner. *Composite Higgs Search at the LHC.* arXiv:1003.3251v1 [hep-ph]

[50] CMS Collaboration. *CMS Physics.* Technical Design Report 8.1, 2006

[51] H. Baer et al.. *Effective Supersymmetry at the LHC.* LPSC10105, UH-511-1152-10, (2010).

[52] M. Bahr et. al.. *Herwig++ Physics and Manual* Eur.Phys.J.C58:639-707, (2008).

[53] J. Alwall, M. Herquet, F. Maltoni, O. Mattelaer, T. Stelzer. *MadGraph 5 : Going Beyond.* JHEP 06 (2011) 128.

[54] The ROOT team. *ROOT - An Object-Oriented Data Analysis Framework.* http://root.cern.ch/root/doc/RootDoc.html 28/03/2012

[55] T. Williams, C. Kelley. *gnuplot 4.6.* http://www.gnuplot.info/documentation.html

[56] S. Frixione and B. R. Webber. *Matching NLO QCD computations and parton shower simulations.* JHEP 0206 (2002) 029.

[57] S. Frixione, P. Nason, and C. Oleari. *Matching NLO QCD computations with Parton Shower simulations: the POWHEG method.* JHEP 0711 (2007) 070.

[58] CMS Collaboration. *Search for new physics with same-sign isolated dilepton events with jets and missing energy.* CMS-PAS-SUS-11-010.

[59] The Durham HepData Project. *Online PDF plotting and calculation.* http://hepdata.cedar.ac.uk/pdf/pdf3.html (2012)

[60] A.D. Martin, W.J. Stirling, R.S. Thorne, G. Watt. *Parton distributions for the LHC.* Eur.Phys.J.C63:189-285, 2009.

[61] Talk given by X. Poveda (ATLAS). *Search for supersymmetry in events involving third generation squarks and sleptons with ATLAS.* http://indico.cern.ch/conferenceDisplay.py?confId=175617 (2012).

[62] CMS Collaboration. *Measurement of the $t\bar{t}$ production cross section in pp collisions at $sqrts = 7$ TeV in dilepton final states containing a τ.* arXiv:1203.6810v1 [hep-ex].

[63] Tevatron Electroweak Working Group, CDF, D0 Collaborations. *Combination of CDF and DO results on the mass of the top quark using up to 5.8 fb-1 of data.* arXiv:1107.5255 [hep-ex].

[64] C. Weiser. *A combined secondary vertex based B-tagging algorithm in CMS.* CERN-CMS-NOTE-2006-014

[65] ATLAS Collaboration. *Calibrating the b -Tag Efficiency and Mistag Rate in 35 pb-1 of Data with the ATLAS Detector.* ATLAS-CONF-2011-089

[66] CMS Collaboration. *Measurement of the b-tagging efficiency using tt events.* CMS PAS BTV-11-003